



**HAL**  
open science

## Uranium Isotope Fractionation in Non-sulfidic Anoxic Settings and the Global Uranium Isotope Mass Balance

Devon B. Cole, Noah J. Planavsky, Martha Longley, Philipp Böning, Daniel Wilkes, Xiangli Wang, Elizabeth D. Swanner, Chad Wittkop, David K. Loydell, Vincent Busigny, et al.

► **To cite this version:**

Devon B. Cole, Noah J. Planavsky, Martha Longley, Philipp Böning, Daniel Wilkes, et al.. Uranium Isotope Fractionation in Non-sulfidic Anoxic Settings and the Global Uranium Isotope Mass Balance. *Global Biogeochemical Cycles*, 2020, 34, p. 201-226. 10.1029/2020GB006649 . insu-03584747

**HAL Id: insu-03584747**

**<https://insu.hal.science/insu-03584747v1>**

Submitted on 24 Jun 2022

**HAL** is a multi-disciplinary open access archive for the deposit and dissemination of scientific research documents, whether they are published or not. The documents may come from teaching and research institutions in France or abroad, or from public or private research centers.

L'archive ouverte pluridisciplinaire **HAL**, est destinée au dépôt et à la diffusion de documents scientifiques de niveau recherche, publiés ou non, émanant des établissements d'enseignement et de recherche français ou étrangers, des laboratoires publics ou privés.

Copyright

# Global Biogeochemical Cycles

## RESEARCH ARTICLE

10.1029/2020GB006649

### Key Points:

- $\delta^{238}\text{U}$  values were measured in iron-rich, anoxic (ferruginous) modern natural environments, and Paleozoic shales deposited under ferruginous conditions
- $\delta^{238}\text{U}$  fractionations in these environments are highly variable and generally indistinguishable from isotopic fractionations associated with oxic settings
- $\delta^{238}\text{U}$  fractionations in these environments are highly variable and generally indistinguishable from isotopic fractionations associated with oxic settings

### Supporting Information:

- Supporting Information S1

### Correspondence to:

D. B. Cole,  
 devon.cole@gatech.edu

### Citation:




Cole, D. B., Planavsky, N. J., Longley, M., Böning, P., Wilkes, D., Wang, X., et al. (2020). Uranium isotope fractionation in non-sulfidic anoxic settings and the global uranium isotope mass balance. *Global Biogeochemical Cycles*, 34, e2020GB006649. <https://doi.org/10.1029/2020GB006649>

Received 28 APR 2020

Accepted 9 JUN 2020

Accepted article online 24 JUN 2020

## Uranium Isotope Fractionation in Non-sulfidic Anoxic Settings and the Global Uranium Isotope Mass Balance

Devon B. Cole<sup>1</sup> , Noah J. Planavsky<sup>2</sup>, Martha Longley<sup>2</sup>, Philipp Böning<sup>3</sup>, Daniel Wilkes<sup>4</sup>, Xiangli Wang<sup>5,6</sup>, Elizabeth D. Swanner<sup>7</sup> , Chad Wittkop<sup>8</sup>, David K. Loydell<sup>9</sup>, Vincent Busigny<sup>10,11</sup> , Andrew C. Knudsen<sup>4</sup>, and Erik A. Sperling<sup>12</sup>

<sup>1</sup>School of Earth and Atmospheric Sciences, Georgia Institute of Technology, Atlanta, GA, USA, <sup>2</sup>Department of Geology and Geophysics, Yale University, New Haven, CT, USA, <sup>3</sup>Institute for Chemistry and Biology of the Marine Environment, University of Oldenburg, Oldenburg, Germany, <sup>4</sup>Department of Geosciences, Lawrence University, Appleton, WI, USA, <sup>5</sup>Department of Marine Science, University of Southern Alabama, Mobile, AL, USA, <sup>6</sup>Dauphin Island Sea Lab, Dauphin Island, AL, USA, <sup>7</sup>Department of Geological and Atmospheric Sciences, Iowa State University, Ames, IA, USA, <sup>8</sup>Department of Chemistry and Geology, Minnesota State University, Mankato, MN, USA, <sup>9</sup>School of the Environment, Geography and Geosciences, University of Portsmouth, Portsmouth, UK, <sup>10</sup>Institut de Physique du Globe de Paris, Sorbonne Paris Cité, University Paris Diderot, Paris, France, <sup>11</sup>Institut Universitaire de France, Paris, France, <sup>12</sup>Department of Geological Sciences, Stanford University, Stanford, CA, USA

**Abstract** Uranium isotopes ( $^{238}\text{U}/^{235}\text{U}$ ) have been used widely over the last decade as a global proxy for marine redox conditions. The largest isotopic fractionations in the system occur during U reduction, removal, and burial. Applying this basic framework, global U isotope mass balance models have been used to predict the extent of ocean floor anoxia during key intervals throughout Earth's history. However, there are currently minimal constraints on the isotopic fractionation that occurs during reduction and burial in anoxic and iron-rich (ferruginous) aquatic systems, despite the consensus that ferruginous conditions are thought to have been widespread through the majority of our planet's history. Here we provide the first exploration of  $\delta^{238}\text{U}$  values in natural ferruginous settings. We measured  $\delta^{238}\text{U}$  in sediments from two modern ferruginous lakes (Brownie Lake and Lake Pavin), the water column of Brownie Lake, and sedimentary rocks from the Silurian-Devonian boundary that were deposited under ferruginous conditions. Additionally, we provide new  $\delta^{238}\text{U}$  data from core top sediments from anoxic but nonsulfidic settings in the Peru Margin oxygen minimum zone. We find that  $\delta^{238}\text{U}$  values from sediments deposited in all of these localities are highly variable but on average are indistinguishable from adjacent oxic sediments. This forces a reevaluation of the global U isotope mass balance and how U isotope values are used to reconstruct the evolution of the marine redox landscape.

## 1. Introduction

The oxygenation of Earth's ocean-atmosphere system marks one of the most dramatic transformations in our planet's history. Quantifying both the magnitude and the timing of this biogeochemical change has been the focus of much work over the last few decades and has major implications for our understanding of the relationship between the evolution of the environment and the biosphere (Cole et al., 2020; Lenton et al., 2014; Sperling, Knoll, & Girguis, 2015). More recently, with the widespread implementation of high-precision analytical techniques, this work has heavily utilized “nontraditional” isotope proxies aimed at reconstructing redox evolution.

Over the last decade, the uranium (U) isotope system ( $^{238}\text{U}/^{235}\text{U}$ ) has emerged as a valuable marine redox proxy, which, when coupled to an isotope mass balance approach, has been used to estimate the global extent of anoxic seafloor area in past oceans (e.g., Bartlett et al., 2018; Brennecke et al., 2011; Clarkson et al., 2018; Elrick et al., 2017; Kendall et al., 2015; Lau et al., 2016, 2017; Lu et al., 2017; Montoya-Pino et al., 2010; Wei et al., 2018; White et al., 2018; Yang et al., 2017; Zhang, Xiao, et al., 2018; Zhang, Algeo, et al., 2018; Zhang, Romaniello, et al., 2018). Because U has a modern marine residence time on the order of ~400,000 kyr (Ku et al., 1977)—orders of magnitude longer than ocean mixing times—the concentration and isotopic composition of U in the open marine system should be relatively homogenous, potentially providing insight about global-scale processes. However, this utility is dependent upon our understanding of

**Table 1**  
*Marine Redox Environments*

Environment	Primary reductant	Modern examples
Euxinic	H <sub>2</sub> S present at high enough levels to build up at or above the sediment–water interface.	Black Sea, Cariaco Basin
Ferruginous	Fe (II) is present, specifically requiring H <sub>2</sub> S-poor conditions	Lake Pavin, Brownie Lake, Lake Matano
Nitrogenous	Neither H <sub>2</sub> S nor Fe (II) rich, oxygen poor, and NO <sub>3</sub> <sup>−</sup> buffered.	Productive regions/upwelling zones such as Peru Margin

U sources and sinks in the modern marine environment and the associated fractionations. The current view of the U isotope system, most simply put, is that heavy U (<sup>238</sup>U) will tend to be preferentially reduced and buried in anoxic settings, while the remaining aqueous phase U will become increasingly isotopically light, due to the nuclear volume effect (NVE; Abe et al., 2008; Abe et al., 2008, 2010; Abe et al., 2014; Basu et al., 2014; Basu et al., 2015; Bigeleisen, 1996a, 1996b; Bigeleisen & Mayer, 1947; Bopp et al., 2010; Fujii et al., 2006; Fujii, Nomura, Okamoto, et al., 1989; Fujii, Nomura, Onitsuka, & Takeda, 1989; Murphy et al., 2014; Nomura et al., 1996; Schauble, 2007; Stirling et al., 2015; Stylo et al., 2015; Wang et al., 2015; Weyer et al., 2008). As a result, at steady-state conditions, an expansion of reducing marine environments should drive a decrease in the δ<sup>238</sup>U value of global seawater.

One of the foremost uncertainties in this framework is that there are no well-defined constraints on the isotopic fractionation of U when removed under iron-rich reducing (ferruginous) conditions (e.g., Gilleaudeau et al., 2019; Hood et al., 2016; Stockey et al., 2020). While these conditions are not present in modern well-oxygenated and sulfate-rich oceans, it is generally accepted that ferruginous environments were widespread through much of Earth's history (e.g., Canfield et al., 2008; Guilbaud et al., 2015; Planavsky et al., 2011; Poulton et al., 2010; Poulton & Canfield, 2011). Specifically, though the extent is debated, Precambrian seas are thought to have been dominated by ferruginous conditions. Indeed, ferruginous reducing environments are thought to have persisted well into the Phanerozoic as evidenced by Sperling, Wolock, et al. (2015), prior to the oxygenation of deep oceans at the end of the Paleozoic (e.g., Lyons & Gill, 2010; Wallace et al., 2017). Even into the Mesozoic, such environments have also been proposed to play a critical role during extinction intervals such as the Permo-Triassic mass extinction (Clarkson et al., 2016), Cretaceous ocean anoxic event (OAE) 2 (März et al., 2008; Poulton et al., 2015), and Cretaceous OAE 3 (März et al., 2008). Finally, while both euxinic and ferruginous environments have been widely observed, reducing but nonsulfidic and iron-poor regions (common in modern high productivity upwelling regions) were likely also a nonnegligible portion of the marine redox landscape (e.g., Frasnian units; Sageman et al., 2003). While we have employed here the redox environment terminology that is broadly used, it is worth noting some of the nuances wrapped into these labels. First, anoxic, ferruginous, and euxinic settings are frequently identified in the rock record using iron speciation (as we have done in this study). However, upon classifying rock samples as being ferruginous, this analysis provides evidence that (1) there was an iron shuttle allowing enrichment of reactive iron below the chemocline and (2) there was enough reactive iron available to control and limit sulfide concentrations. This analysis does not *necessarily* demonstrate that there were high concentrations of Fe (II) in the water column. As a result, such an environment observed in a modern setting might instead be classified as anoxic but nonsulfidic, or nitrogenous (see Table 1). Providing distinction between these environments in the rock record and adjusting terminology in the broader community are beyond the scope of this work; however, our investigation of a suite of anoxic but nonsulfidic modern redox environments herein provides useful insight for the behavior of U in a range of likely common redox environments of the past.

Uranium has two primary valence states in surface environments—soluble U (VI) and relatively insoluble U (IV). The <sup>238</sup>U/<sup>235</sup>U (reported relative to the CRM 112a standard, minus 1, and multiplied by 1,000; denoted δ<sup>238</sup>U) system is dominantly fractionated during biotically mediated reduction of U (VI) to U (IV). This process generally results in the preferential reduction of <sup>238</sup>U due to NVE (e.g., Bigeleisen, 1996a; Nomura et al., 1996; Schauble, 2007) and the subsequent isotopic enrichment of reduced species. However, some experimental studies have observed—in the presence of iron (Fe) as a reductant—either no fractionation as a result of near-quantitative reduction (Du et al., 2011) or preference for the light isotope during abiotic reduction (e.g., Rademacher et al., 2006; Stylo et al., 2015), the latter of which may be consistent with

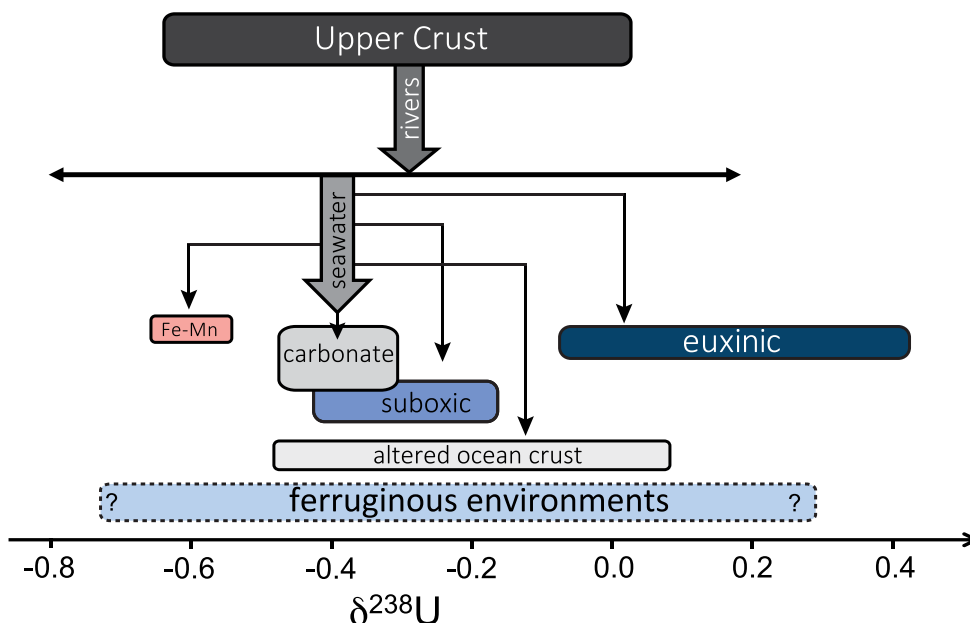


**Figure 1.** A schematic of the uranium isotope mass balance in Earth's surface reservoirs. Fractionations from seawater are based on modern observations. Reducing environments in blue, including a separate ferruginous sink, which is currently unconstrained and critical for understanding past oceans (adapted from Andersen et al., 2017; Tissot & Dauphas, 2015).

mass-dependent fractionation (MDF) effects. Further, it has recently been shown that abiotic fractionation is primarily controlled by aqueous speciation of U and the rate of removal, which dictates the relative expression of NVE and MDF effects (Brown et al., 2018). Regardless of the pathway, once reduced, relatively insoluble U (IV) is removed from the aqueous system, and the isotopic signature can be recorded in sediments. However, the magnitude of the observed isotopic shift between the aqueous system and the sedimentary record is controlled not only by the extent of reducing environments but also by the mechanism of reduction, associated U isotopic fractionation factors, and U mass accumulation rates (UMARs; e.g., Andersen et al., 2016; Brown et al., 2018; Lau et al., 2020; Tissot & Dauphas, 2015).

### 1.1. Global Uranium Isotope Mass Balance

The dominant source of U to the marine system is riverine input, which directly reflects crustal composition. While it has been observed that there is some riverine variability (e.g., Yangtze river; Andersen et al., 2016), the mean value is isotopically indistinguishable from that of the upper crust with a  $\delta^{238}\text{U}$  value of approximately  $-0.29 \pm 0.06\text{‰}$  (Andersen et al., 2017; Tissot & Dauphas, 2015). As a result, the isotopic composition of seawater is controlled by both the magnitude (UMAR) and associated isotopic fractionation of various removal pathways (Figure 1). In the modern oceans, the dominant sinks for U are removal in reducing environments, incorporation into carbonate sediments, sorption onto Fe-Mn oxides, and hydrothermal alteration of basalts (Dunk et al., 2002). Authigenic reduced U found in sediments deposited under euxinic conditions has the heaviest  $\delta^{238}\text{U}$  values, with a mean of  $-0.03 \pm 0.04\text{‰}$  or an average isotope fractionation ( $\Delta^{238}\text{U}$ ;  $\delta^{238}\text{U}_{\text{euxinic}} - \delta^{238}\text{U}_{\text{seawater}}$ ) from seawater of  $\sim 0.4\text{‰}$  (mean modern seawater [ $\delta^{238}\text{U}_{\text{seawater}}$ ] has an isotopic composition of  $-0.39 \pm 0.02\text{‰}$ ) (Andersen et al., 2014, 2015, 2016; Tissot & Dauphas, 2015; Weyer et al., 2008). In reducing settings not rich in sulfide or ferrous iron (often referred to as suboxic environments; nitrogenous, see Table 1; Canfield & Thamdrup, 2009), such as modern highly productive coastal upwelling regions, fractionations from seawater are less pronounced with mean  $\delta^{238}\text{U}$  of  $-0.24 \pm 0.8\text{‰}$  (Andersen et al., 2016; Weyer et al., 2008). In contrast, U removed via sorption onto Fe and Mn oxyhydroxides as observed in marine iron-manganese crusts will be preferentially light with a mean  $\delta^{238}\text{U}$  of  $-0.64 \pm 0.02\text{‰}$  (Andersen et al., 2016; Brennecke et al., 2011). It should, however, also be noted that no isotopic effects have been reported as a result of adsorption-desorption reactions in groundwaters (Shiel et al., 2016).

Our understanding of the U isotope mass balance in the modern ocean is relatively well constrained (e.g., Dunk et al., 2002; Tissot & Dauphas, 2015). However, the redox environment of the marine system has changed substantially through Earth's history, and a more nuanced understanding of U behavior in various reducing sinks is necessary to draw reasonable conclusions about the extent of these environments in the past. This is especially vital since reducing environments would have been considerably more widespread than today, thus amplifying errors on assumed values for both UMAR and U isotopic fractionation factors.

Traditional U isotope mass balance models simplify all types of reducing environments as “anoxic settings”; however, there are likely substantial differences in both the fractionation factor ( $\Delta^{238}\text{U}$ ) and UMAR associated with reduction in euxinic, ferruginous, and anoxic but reductant poor settings—yet all but the first remain poorly understood. While these simplifications are reasonable and useful for modern-like oceans given dominantly oxygenated conditions and abundant sulfate, this approach becomes fundamentally flawed moving back in time to intervals with widespread anoxia. Foremost, reducing environments during many periods of the Proterozoic, Paleozoic, and Mesozoic were most likely dominated by ferruginous conditions (e.g., Clarkson et al., 2018; Planavsky et al., 2011; Poulton & Canfield, 2011; Sperling, Wolock, et al., 2015), and again, these settings remain virtually uncharacterized with regard to U cycling. Further, it is also likely that even in intervals characterized by relatively large swaths of euxinic conditions (e.g., the early Silurian or the middle Devonian; e.g., Meyer & Kump, 2008; Stockey et al., 2020), noneuxinic but anoxic environments were still important components of the redox landscape (e.g., Rimmer, 2004; Sageman et al., 2003).

In order to refine our understanding of the U isotope mass balance, we provide new constraints on the isotopic fractionation associated with U burial under ferruginous conditions. We combine data from two modern ferruginous lakes that have been used as analogs for reducing marine settings in Earth's early oceans, as well as U isotope data from a range of Paleozoic siliciclastic sections that have been independently constrained as deposited under ferruginous conditions based on Fe speciation. In addition, we explore U isotope signatures through and below the oxygen minimum zone (OMZ) within the Peru Margin upwelling zone to characterize a second unique type of nitrate-reducing environment poor in both ferrous iron and sulfide, which may also have been very common in past oceans.

## 2. Geologic Settings

### 2.1. Modern Environments

#### 2.1.1. Brownie Lake

Brownie Lake is a permanently redox-stratified, iron-rich lake located in Minneapolis, MN, USA (Lambrecht et al., 2018; Tracey et al., 1996). The lake is characterized in detail by Lambrecht et al. (2018). The lake has a maximum depth of ~14 m, with a chemocline at ~4–5 m. Below the chemocline, dissolved Fe (II) has been observed up to ~1,500  $\mu\text{M}$  (Lambrecht et al., 2018). Dissolved  $\text{O}_2$  concentrations were below detection limits below 4 m depth (Lambrecht et al., 2018). Dissolved inorganic carbon (DIC) averaged ~1.6 mM at 1 m depth and ~13.2 mM at 13 m depth, while pH ranges from 8.85 at 1 m depth to 6.86 at 14 m depth. Carbonate ion concentrations were calculated to be 83.88  $\mu\text{M}$  at 1 m depth and 20.25  $\mu\text{M}$  at 13 m depth. Bicarbonate ion concentrations were calculated to be 1,604.44  $\mu\text{M}$  at 1 m depth and 10,877.20  $\mu\text{M}$  at 13 m depth (see supporting information (SI) for data used in calculations). Sulfate concentrations are low, measured at ~50  $\mu\text{M}$  at 1 m depth and ~1  $\mu\text{M}$  (just above detection limits) at 13 m depth (Lambrecht et al., 2018). Significantly, these sulfate concentrations are at the lower end of levels commonly estimated for the Proterozoic and Paleozoic (e.g., Fakhraee & Katsev, 2019), making these conditions a reasonable analog for what are thought to be widespread ferruginous conditions in Paleozoic and Precambrian seas. It should, however, be noted that while marine iron concentrations of Earth's early oceans are poorly constrained (estimated to be between 500 nM and 500  $\mu\text{M}$ ; Halevy et al., 2017; Holland, 1984), relative to sulfide, Fe (II) would have been the primary reductant in what are described as ferruginous seas.

At Brownie Lake, two cores were taken: the first at ~3 m depth (above the chemocline; oxygenated bottom waters) and the second at 14 m depth (below the chemocline; anoxic and Fe-rich bottom waters). Water samples were also collected through the water column every 0.5–1 m to the maximum depth of 13 m. Uranium isotopes and trace metal contents were analyzed in bulk sediments throughout both cores and the water column (see below).

### 2.1.2. Lake Pavin

Similar to Brownie Lake, Lake Pavin is a permanently redox-stratified lake with anoxic, iron-rich deep waters located in central France. The lake has a maximum depth of ~92 m and a chemocline at ~60 m. Dissolved Fe (II) concentrations reach up to 1,200  $\mu\text{M}$  below the chemocline, and sulfate concentrations are ~15  $\mu\text{M}$  above the chemocline and decrease to <1  $\mu\text{M}$  below the chemocline (Busigny et al., 2014; Busigny et al., 2016; Michard et al., 1994; Viollier et al., 1995). The pH in Lake Pavin is ~8.06 at 1 m depth and steadily decreases to ~6.03 at 88 m depth, while DIC is ~0.4 mM at 1 m depth and ~16 mM at 88 m depth (Michard et al., 1994). Carbonate ion concentrations were calculated to be 7.46  $\mu\text{M}$  at 1 m depth and 1.03  $\mu\text{M}$  at 90 m depth. Bicarbonate ion concentrations were calculated to be 385.88  $\mu\text{M}$  at 1 m depth and 5,642.71  $\mu\text{M}$  at 90 m depth (see SI). Unfortunately, waters from Lake Pavin were not analyzed for U isotopes, as water column concentrations of U are very low (Viollier et al., 1995).

At Lake Pavin, U isotopes were analyzed in bulk sediments from the four cores studied by Busigny et al. (2014), including a core at 32 m (above the chemocline), cores at 60 and 65 m (within the chemocline), and a core at 92 m (below the chemocline; deepest point of the lake). Uranium isotopes and trace metal contents were analyzed for bulk sediments in the upper portions of these cores, which are the same samples used and described by Busigny et al. (2014).

### 2.1.3. Peru Margin

The Peru Margin hosts a highly productive perennial upwelling zone between 7°S and 20°S, directly off the coast of Peru in the east Pacific. The high productivity of this region results in an OMZ with  $\text{O}_2 < 5 \mu\text{M}$  between water depths of ~50–650 m (Lückge & Reinhardt, 2000) on the shelf and slope, with the core of the OMZ (150–400 m depth) becoming fully anoxic with  $\text{O}_2 < 10 \text{ nM}$  (Revsbech et al., 2009; Thamdrup et al., 2012). High sulfate concentrations in the modern ocean tend to result in the predominance of sulfate reduction in low oxygen settings and organic rich sediments, as well as the rapid formation of iron sulfides upon the reduction of iron oxyhydroxides. However, the Peru Margin is dominantly characterized by nitrogenous (nitrate-reducing) conditions, as well as high concentrations of dissolved iron (~50–75 nmol/L), where most of the iron below the oxycline is present as Fe (II) (Vedamati et al., 2014). The underlying anoxic sediments are the primary source of this iron and have been shown to have the highest measured Fe (II) flux from sediments of any similar modern ocean margin environment with depleted  $\text{O}_2$  (Noffke et al., 2012; Plass et al., 2019; Scholz et al., 2016). Reduction is thought to occur largely in pore waters; however, there is also evidence of an Fe particulate shuttle associated with the accumulation of Mo in the sediment column (Scholz et al., 2017). While this setting cannot be described as ferruginous, it is, in large parts, fully anoxic (Revsbech et al., 2009; Thamdrup et al., 2012) and represents a dynamic open-marine anoxic environment, with reduction pathways not previously characterized for U isotopic signatures.

On the Peru Margin, U isotopes and trace metal contents were measured in bulk sediment in core top samples from a set of cores recovered during cruise 147 of R/V *Sonne* (Kudrass, 2000) subsequently analyzed by Böning et al. (2004). These cores were taken from the upper edge of the OMZ (bottom water  $\text{O}_2$  is typically <10  $\mu\text{M}$ , with some variability under El Niño conditions; e.g., Gutiérrez et al., 2008), within the OMZ (bottom water  $\text{O}_2 < 5 \mu\text{M}$ ), and below the OMZ (bottom water  $\text{O}_2 > 10 \mu\text{M}$ ) as recorded at the time of collection (Böning et al., 2004; Lückge & Reinhardt, 2000). Although the oxygen concentrations may appear relatively high, this is likely a feature of detection limits during the collection of these samples. Measurements could be further complicated by the highly variable  $\text{O}_2$  concentrations of waters overlying the samples from the upper edge of the OMZ (e.g., Scholz et al., 2016, 2017). Regardless, the rest of the OMZ samples fall largely within the fully anoxic core of the OMZ which has  $\text{O}_2 < 10 \text{ nM}$  (below the detection limit of STOX sensors), as more recently documented by Revsbech et al. (2009); Thamdrup et al. (2012).

## 2.2. Paleozoic Environments

### 2.2.1. Road River Group—Tetlit Creek

The Road River Group is located in the northern Canadian Cordillera of the Yukon and records deep-water deposition through much of the Paleozoic. Here we focus on the upper portion of the Group from the type section at Tetlit Creek (Jackson & Lenz, 1962), which represents the upper Silurian through Lower Devonian. These samples correspond directly to meter heights in Table 1 of Lenz (1988), which constrains the age of the samples. Specifically, the Lenz (1988) biostratigraphic study places the base of the investigated section in the Ludlow and the upper boundary in the Pragian (Lenz, 1988). This section is dominated by

unbioturbated calcareous organic-rich shale (average weight percent total organic carbon [TOC] of samples from the section was  $3.0 \pm 1.9$  weight percent; average mass loss on acidification, i.e., weight percent carbonate was  $35 \pm 15$  weight percent). All samples analyzed were devoid of evidence for surface weathering.

### 2.2.2. Additional Graptolitic Shale Samples

Additional graptolite samples from the collections of Dr. Alf Lenz (University of Western Ontario) and Dr. David Loydell (University of Portsmouth) were also analyzed. Twelve samples are from the Cape Phillips Formation at the Twilight Creek section, Nunavut, Canada, and span a similar upper Silurian-Lower Devonian (Přidolí – Pragian) interval to the Tetlit Creek samples (samples correspond to Figure 4 of Lenz, 2013). An additional 19 samples (16 Silurian and 3 Ordovician; for more details, see SI) come from a number of different localities globally; despite a lack of contextual  $\delta^{238}\text{U}$  data within a stratigraphic section, these samples provide additional data solely as a record of  $\delta^{238}\text{U}$  values possible in sediments constrained as deposited in ferruginous conditions.

## 3. Methods

### 3.1. Water Samples

The water samples from Brownie Lake were collected during the same sampling campaign as the sediment samples in May 2017 (Lambrecht et al., 2018). Waters were collected with a Proactive Mini Monsoon pump with a low-flow controller and vinyl tubing and then filtered with a syringe filter (0.2  $\mu\text{m}$ ) directly attached to tubing, as described by Lambrecht et al. (2018). The filtered water samples were collected into acid-cleaned plastic bottles and then acidified to  $\text{pH} < 2$  using concentrated HCl to redissolve any species that may have precipitated as a result of oxidation.

### 3.2. Sediment Samples

All sediment analyses were conducted on bulk sediment digests. Brownie Lake samples were dried at  $100^\circ\text{C}$  for 24 hr to remove any remaining water and then ashed at  $600^\circ\text{C}$  for 12 hr to remove organic matter. Graptolitic shale samples were prepared first by removing any weathered surfaces using a diamond-edge rock saw and then powdered in an agate or tungsten carbide mill. The powders were then ashed at  $600^\circ\text{C}$  for 12 hr to remove organic matter prior to dissolution. Sample powders from Lake Pavin are from the same sample set as that prepared by Busigny et al. (2014), while samples from the Peru Margin are from those prepared and analyzed by Böning et al. (2004).

Powders from all sampling localities were dissolved using a three-acid dissolution method for total dissolution of each sample. Nitric and hydrofluoric acids were added in excess of samples to dissolve for a minimum of 12 hr at  $105^\circ\text{C}$ . Samples were then dried down and subjected to a second dissolution step using aqua regia for a minimum of 12 hr at  $105^\circ\text{C}$ . Finally, samples were dried down and then redissolved in 5 ml 6 N HCl for storage and analysis.

### 3.3. Iron Speciation and Carbon Analyses

Sequential iron extraction methods were used to isolate Fe in carbonate, (oxyhydr)oxides, and mixed valence state pools using the methods of Poulton and Canfield (2005). The iron extracted in each step was quantified using the ferrozine method of Stookey (1970). Iron in the pyrite phase ( $\text{Fe}_{\text{Py}}$ ) was extracted using the chromium reducible sulfur (CRS) method defined in Canfield et al. (1986). These phases make up the highly reactive iron ( $\text{Fe}_{\text{HR}}$ ) pool. Based on calibration in the modern ocean, samples are considered anoxic when  $\text{Fe}_{\text{HR}}/\text{Fe}_{\text{T}} > 0.38$  (Raiswell & Canfield, 1998). These anoxic environments can either be characterized by abundant sulfide (euxinic) or abundant Fe (II) (ferruginous). These two endmembers can be distinguished by the ratio of  $\text{Fe}_{\text{Py}}$  (Fe extracted during CRS) to  $\text{Fe}_{\text{HR}}$ . When  $\text{Fe}_{\text{Py}}/\text{Fe}_{\text{HR}} < 0.7\text{--}0.8$ , this is indicative of deposition in ferruginous environments (Anderson & Raiswell, 2004; März et al., 2008; Poulton & Canfield, 2011).

Mass loss on acidification (weight percent carbonate) was quantified by acidifying  $\sim 1$  g of sediment overnight with 3 N HCl, washing and drying the residue, and reweighing the pellet. TOC contents were measured on an NC Technologies ECS 8020 Elemental Analyzer at Stanford University.

### 3.4. Elemental Concentrations

Major and trace elements for total digests were analyzed in the Yale Metal Geochemistry Center by ICP-MS (Element XR, Thermo-Finnigan) using a standard sample introduction system and following the methods of

Gueguen et al. (2016). For sediment samples, an aliquot of the 6 N HCl stock solutions obtained after total digests was diluted in 5% HNO<sub>3</sub>, and U, Th, and Fe were measured in medium resolution. Measurement precision was generally better than 5% and the USGS geostandards BHVO-2, Nod A-1, and Brush Creek Shale processed along with samples during each run are within 10% of reported values. For the water samples, U concentrations reported use the isotope dilution method after double-spiking and separation for isotope analyses (see below).

### 3.5. Uranium Isotope Analyses

Uranium was separated from waters and sediments using the same <sup>233</sup>U-<sup>236</sup>U double spike method with UTEVA ion exchange resin (see methods of Wang et al., 2016; Weyer et al., 2008). Double spike was added to samples prior to column chemistry in an amount based on previous measurement of U concentrations to achieve a <sup>238</sup>U/<sup>236</sup>U ratio of ~30. Samples were then evaporated to dryness and brought up in 3 N HNO<sub>3</sub>. Samples were then purified on UTEVA resin columns using the method of (Wang et al., 2016). Dependent on sample concentration, 100–40 ng were loaded on columns. After purification, U samples were dissolved in 0.3 N HNO<sub>3</sub> to achieve 50 ppb solutions for analysis. Samples were measured on a Thermo-Finnigan Neptune Plus Multi-Collector ICP-MS at the Yale Metal Geochemistry Center. Samples were introduced using an ApexIR sample introduction system and measured at low resolution. Isotopes <sup>232</sup>Th, <sup>233</sup>U, <sup>235</sup>U, <sup>236</sup>U, and <sup>238</sup>U were measured simultaneously on Faraday collectors connected to 10<sup>11</sup> Ω amplifiers achieving a signal of ~25–45 volts on <sup>238</sup>U, dependent on concentration.

The CRM 112a (New Brunswick Laboratory, U.S. Department of Energy) standard was analyzed every three samples to monitor drift in instrumental performance, accuracy, and precision, and samples were normalized to the average of bracketing standards. Standard concentration was matched to sample concentrations to maintain similar voltage. The drift of the standard was less than 0.07‰. Blank levels were always less than 0.1% of sample voltage, and no blank correction was made as this would be smaller than the instrumental counting error. External reproducibility was 0.1‰ based on analyses of both the USGS geostandard Nod A-1 (−0.55 ± 0.1‰ (2SD), *n* = 12) and sample duplicates (*n* = 16). Water samples were measured alongside the Atlantic Seawater standard (OSIL) (−0.33 ± 0.06‰ [2SD], *n* = 2). The concentration of U was calculated using the isotope dilution method, and precision was ~1%.

Authigenic  $\delta^{238}\text{U}$  values in sediments ( $\delta^{238}\text{U}_{\text{auth}}$ ) were estimated for both lakes and Paleozoic data sets. The calculated  $\delta^{238}\text{U}_{\text{auth}}$  values estimate the detrital contribution of U based on the crustal average U/Th of Rudnick and Gao (2014), with error bars calculated based on the confidence intervals for detrital U/Th of Cole et al. (2017). No corrections were made for samples with less than 35% higher U/Th than crustal average to avoid propagation of large correction errors.

## 4. Results

### 4.1. Modern Environments

#### 4.1.1. Brownie Lake

In the oxic and anoxic cores at Brownie Lake, we find overlapping ranges of  $\delta^{238}\text{U}$  values. The  $\delta^{238}\text{U}_{\text{auth}}$  values in the anoxic core range from −0.35‰ to 0.64‰ with a mean of  $-0.07 \pm 0.59\%$  (2SD), while the oxic core ranges from −0.31‰ to −0.02‰ with a mean of  $-0.15 \pm 0.18\%$  (2SD) (Figure 2). Uranium enrichments are also highly variable with U/Th ranging from 0.11 to 1.57 (ppm/ppm) with a mean of  $0.56 \pm 0.38$  and  $0.89 \pm 0.89$  in the anoxic and oxic cores, respectively (Figure 2). We observe an apparent relationship between the  $\delta^{238}\text{U}_{\text{auth}}$  values in the upper 10 cm of the two cores, with the anoxic core consistently averaging ~0.1‰ lighter than the oxic core; however, these values are nearly all within error and therefore not significant (Figure 3). Below 15 cm,  $\delta^{238}\text{U}_{\text{auth}}$  values in the anoxic core become very heavy (up to 0.64‰) and then return to scattered values similar to the upper portion, while the oxic core remains less variable.

In the water column samples,  $\delta^{238}\text{U}$  above the chemocline averages  $-0.16 \pm 0.12\%$ , while below the chemocline, the mean is  $-0.41 \pm 0.26\%$  (Figure 4). The U concentration in the water column is higher in the surface waters (averaging  $1.17 \pm 0.4$  ppb) than below the chemocline (averaging  $0.56 \pm 0.6$  ppb). Significantly, there are no trends in U concentration coincident with the chemocline; however, concentrations do decrease where iron concentrations begin to increase. Similarly,  $\delta^{238}\text{U}$  values show a shift to lighter values between six and seven meters depth—just below the chemocline—where iron concentrations begin to increase.



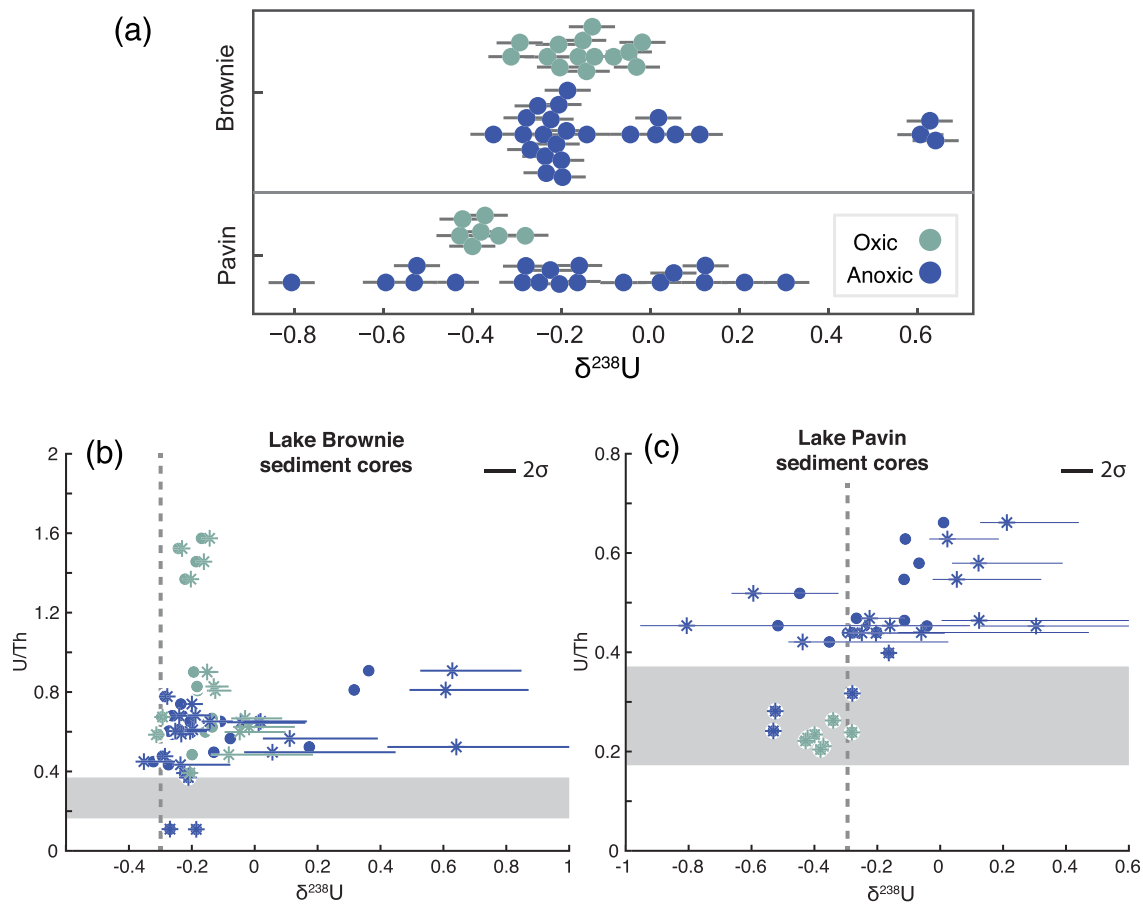


**Figure 2.**  $\delta^{238}\text{U}$  data from modern ferruginous Brownie Lake and Lake Pavin. Data from anoxic cores in blue, oxic in green. (a) Spread of  $\delta^{238}\text{U}_{\text{auth}}$  data from both lakes. (b, c)  $\delta^{238}\text{U}$  plotted against U/Th for Lake Brownie and Lake Pavin, respectively. Circles represent original data, while stars show  $\delta^{238}\text{U}_{\text{auth}}$  with error bars calculated based on confidence intervals for crustal input from Cole et al. (2017). Crustal confidence intervals for U/Th shown by gray bars. Uranium isotopic composition of crust shown by dashed lines.

Below this level, the trend reverses back toward heavier  $\delta^{238}\text{U}$  values. We also compare the water column  $\delta^{238}\text{U}$  to the  $\delta^{238}\text{U}$  from the top 10 cm of both sediment cores. We have chosen this comparison since sediment values appear most consistent and show related trends, given that the water residence time is extremely short (2 years; Minneapolis Parks & Recreation Board, 2017). The mean  $\delta^{238}\text{U}_{\text{auth}}$  from this upper portion of the oxic core is  $-0.15 \pm 0.13\text{‰}$ , while the mean  $\delta^{238}\text{U}_{\text{auth}}$  from the upper portion of the anoxic core is  $-0.26 \pm 0.1\text{‰}$ . While these means are both within 2SD, the water  $\delta^{238}\text{U}$  above the chemocline is nearly identical to that of the oxic core, while the water below the chemocline is slightly lighter (although still within 2SD).

#### 4.1.2. Lake Pavin

In Lake Pavin, the range of  $\delta^{238}\text{U}_{\text{auth}}$  is relatively limited in the oxic core, ranging from  $-0.43\text{‰}$  to  $-0.28\text{‰}$  with a mean of  $-0.37 \pm 0.10\text{‰}$ , while cores from just below the chemocline and the lake bottom range from  $-0.81\text{‰}$  to  $0.30\text{‰}$  with a mean of  $-0.19 \pm 0.59\text{‰}$  (Figure 2). U/Th ratios range from 0.20 to 0.66 with a weak positive correlation with  $\delta^{238}\text{U}$  ( $R^2 = 0.30$ ) and a mean of  $0.23 \pm 0.04$  in the oxic sediments and a mean of  $0.45 \pm 0.21$  in the anoxic sediments (Figure 2). There are no distinct trends repeated across all four cores (Figure 3); however, both cores at the chemocline have increasingly light values with core depth.

#### 4.1.3. Peru Margin

Core top samples from the Peru Margin from the upper edge of the OMZ and through the OMZ have  $\delta^{238}\text{U}$  values ranging from  $-0.27\text{‰}$  to  $-0.08\text{‰}$  with a mean of  $-0.20 \pm 0.12\text{‰}$ , while samples from sediments underlying oxygenated waters below the OMZ range from  $-0.39\text{‰}$  to  $-0.25\text{‰}$  with a mean of  $-0.32 \pm 0.12\text{‰}$  (Figure 5). These sediments are less variable overall than those recovered from the

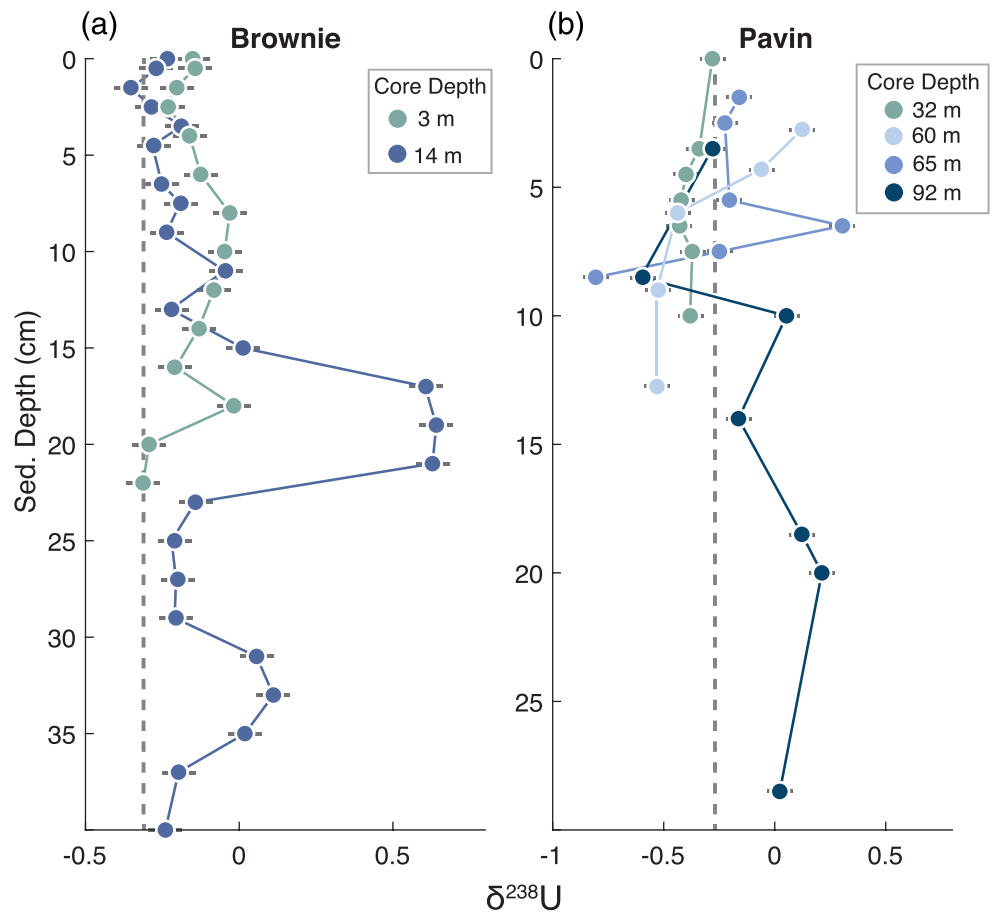


**Figure 3.** Core depth profiles for (a) Brownie and (b) Pavin. Cores sampled above the chemocline are shown in green (3 m depth at Brownie, 32 m depth at Pavin). Blue shows cores from at or below the chemocline (14 m depth at Brownie, 60, 65, and 92 m at Pavin with darker colors indicating deeper cores). Dashed lines represent crustal  $\delta^{238}\text{U}$  composition.

ferruginous lakes; however, isotopic signatures from within versus below the OMZ are within uncertainty. Similar to the isotopic data, U/Th concentrations do not show a significant shift within the OMZ (mean of  $3.53 \pm 2.56$ ) relative to more oxygenated waters (mean  $1.53 \pm 2.28$ )—although the mean value is higher, both groups are within 2SD. In contrast, TOC data show a significant increase within the OMZ (mean of  $19.13 \pm 5.13$  wt%) compared to more oxygenated waters (mean of  $6.46 \pm 3.81$  wt%). We find a distinct covariation between U/Th and TOC ( $R^2 = 0.54$ ,  $p = 1.08 \times 10^{-5}$ ). Finally, we observe no isotopic trends tied to the location of core tops within or at the upper edge of the OMZ.

#### 4.2. Paleozoic

Paleozoic samples were specifically selected to represent deposition in ferruginous environments based on iron speciation data (see SI). Samples were selected based on filtering for ferruginous conditions based on Poulton and Canfield (2011). These samples are composed of both a single continuous section of the Road River Group at Tetlit Creek and additional graptolite collection samples from a range of localities. Broadly, we find similar trends in both groups of Paleozoic samples—namely, major variability in  $\delta^{238}\text{U}$  values, a weak correlation of  $\delta^{238}\text{U}$  values with U/Th, and a positive relationship with TOC.

##### 4.2.1. Road River Group

Samples from the Tetlit Creek section of the Road River Group have  $\delta^{238}\text{U}$  values ranging from  $-0.64\text{‰}$  to  $0.36\text{‰}$  with a mean of  $-0.09 \pm 0.49\text{‰}$  (Figure 6), while U/Th values are highly variable and range from 0.51 to 19.27 with a mean of  $4.54 \pm 9.90$  (Figure 6). These samples are also relatively rich in TOC, with values ranging from 0.3–6.4 wt% with a mean of 2.74 wt% (Figure 6). There is an apparent weak positive correlation

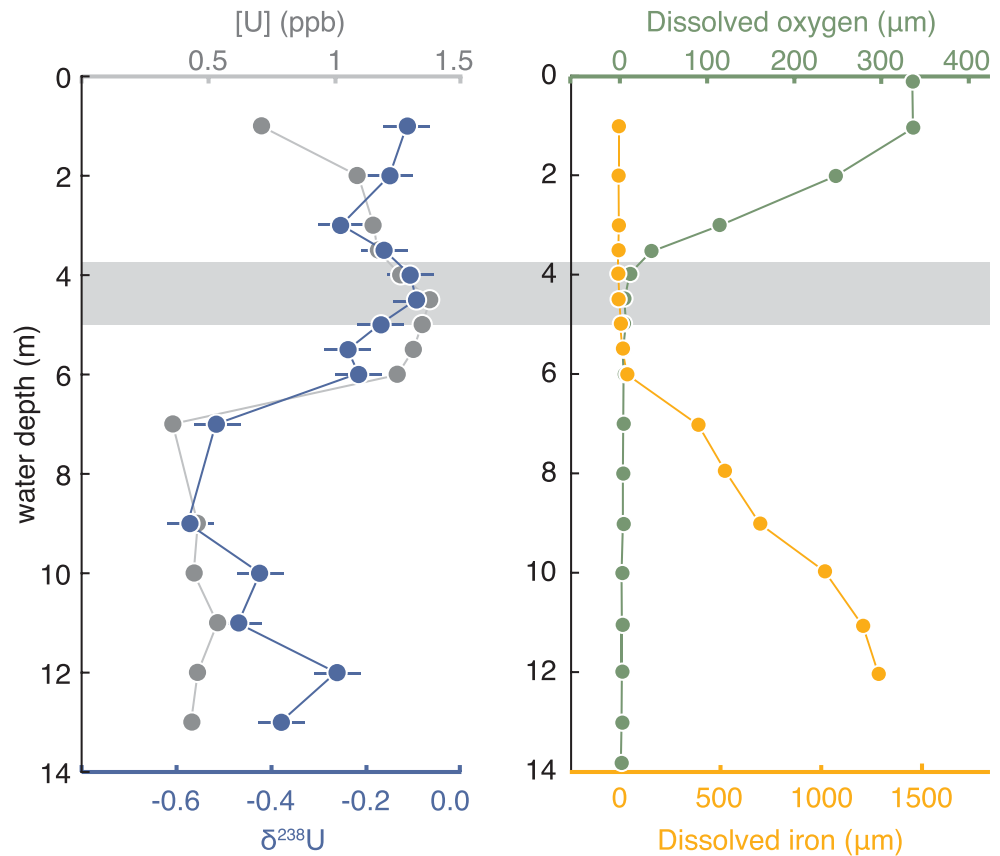


**Figure 4.** Brownie Lake water column data. (a)  $\delta^{238}\text{U}$  and  $[\text{U}]$  data as a function of depth. (b) Dissolved oxygen and iron as a function of depth; May 2017. Chemocline represented by the gray bar.

between  $\text{U}/\text{Th}$  and  $\delta^{238}\text{U}$  ( $R^2 = 0.17$ ,  $p = 6.2 \times 10^{-4}$ ). We find a stronger correlation between  $\text{TOC}$  and  $\delta^{238}\text{U}$  ( $R^2 = 0.30$ ,  $p = 4.8 \times 10^{-7}$ ).

#### 4.2.2. Additional Graptolite Samples From ~460–428 Ma

Similar to the samples from the Road River Group,  $\delta^{238}\text{U}$  values range from  $-0.68\text{‰}$  to  $0.18\text{‰}$  with a mean of  $-0.15 \pm 0.40\text{‰}$ , while  $\text{U}/\text{Th}$  values are highly variable with a mean of  $8.30 \pm 14.82$ , showing a similar range and relationship with  $\delta^{238}\text{U}$  ( $R^2 = 0.14$ ,  $p = 5.9 \times 10^{-5}$ ) as that observed in the samples from the Road River Group (Figure 7). These samples have  $\text{TOC}$  values ranging from 0.17–5.33 wt% with a mean of 2.25 wt%. Even more so than the Road River, we find a stronger correlation between  $\text{TOC}$  and  $\delta^{238}\text{U}$  in these samples ( $R^2 = 0.45$ ,  $p = 1.5 \times 10^{-10}$ ). Combining both the Road River and additional graptolitic samples, we find that the relationship between  $\delta^{238}\text{U}$  and  $\text{TOC}$  is most important ( $R^2 = 0.44$ ,  $p = 1.5 \times 10^{-16}$ ) (Figure 7).

## 5. Discussion

### 5.1. Ferruginous Lakes

We find that, in the examined ferruginous lakes,  $\delta^{238}\text{U}$  values from the oxic cores are statistically indistinguishable from the anoxic cores (Figure 2). However, the  $\delta^{238}\text{U}$  values from the oxic cores in both lakes show substantially less variability than the anoxic cores, which range more than  $1\text{‰}$ , roughly equivalent to the average range of fractionations observed in Earth's sedimentary rock record (Figure 1) (Wang et al., 2018), although it should be noted that fractionations up to  $5\text{‰}$  in nonsedimentary material have been measured (Basu et al., 2015; Hiess et al., 2012; Murphy et al., 2014; Stirling et al., 2007). Further, the  $\delta^{238}\text{U}$  values in the anoxic cores are not only highly variable—they also include values both lighter and heavier than those of the sediments from the oxic core, as well as the water column. This indicates that multiple reduction pathways are present—likely combined with varied expression of fractionation factors—resulting in a range of isotopic effects. Both lakes have lower concentrations of carbonate ion than seawater ( $\sim 200 \mu\text{mol}/\text{kg}$ )—especially

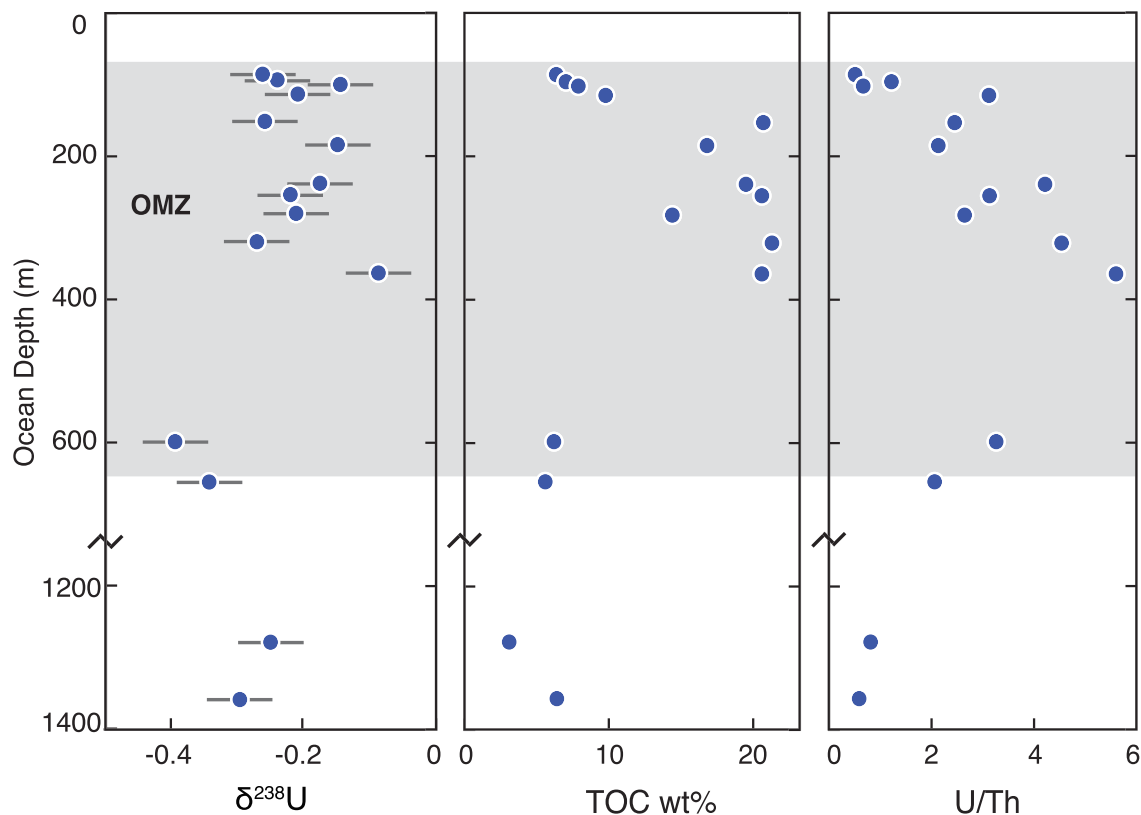


**Figure 5.**  $\delta^{238}\text{U}_{\text{auth}}$ , TOC, and U/Th data from core tops through the Peru Margin OMZ. The gray bar represents the OMZ, while waters above and below this region are oxygenated. TOC data from Böning et al. (2004). Data points for TOC and U/Th are larger than the error on these measurements.

Lake Pavin, and we note that pH is substantially lower in anoxic versus oxic waters, while DIC is substantially higher. However, we do not expect significant changes in U speciation above and below the chemocline. Lastly, while we do not currently have constraints on the balance between pore water and water column reduction, we note that this would be a promising avenue for future work.

#### 5.1.1. Brownie Lake

In Brownie Lake, the anoxic core is consistently lighter than the oxic core in the upper ~10 cm (Figure 3), which suggests preferential removal of the light isotope ( $^{235}\text{U}$ ) to the sediment—the opposite of what is traditionally expected in anoxic settings, and providing evidence in a natural setting for the expression of kinetic MDF effects (Brown et al., 2018). Despite this, the water  $\delta^{238}\text{U}$  values also show an isotopic shift toward lighter values just below the chemocline. While there may be small amounts of heavier U being removed from the water column, there is no evidence of substantial and significant isotopic fractionations associated with U cycling in this setting.

Beyond our key observation that U reduction in this ferruginous environment does not conform with the conventional understanding of U isotope behavior, we highlight below a number of processes relevant to this system and their relationship with our data.

First, in the anoxic core, below the upper 10 cm, there is a jump to heavier  $\delta^{238}\text{U}$  values; however, there is no correlated shift in U/Th ratios, suggesting that the observed fractionation is not tied to an increase in removal efficiency (UMAR). Potentially, this larger apparent isotopic fractionation could be tied to a more complete expression of intrinsic fractionation factors—resulting from a shift to reduction in the water column (a non-diffusion-limited setting) (e.g., Clark & Johnson, 2008). Unfortunately, given the extremely short residence time of Brownie Lake waters, such hypotheses are difficult to support.

Second, the heavier  $\delta^{238}\text{U}$  values observed are most similar to what would be expected in euxinic settings (e.g., the Black Sea; Andersen et al., 2014; Montoya-Pino et al., 2010; Rolison et al., 2017; Weyer

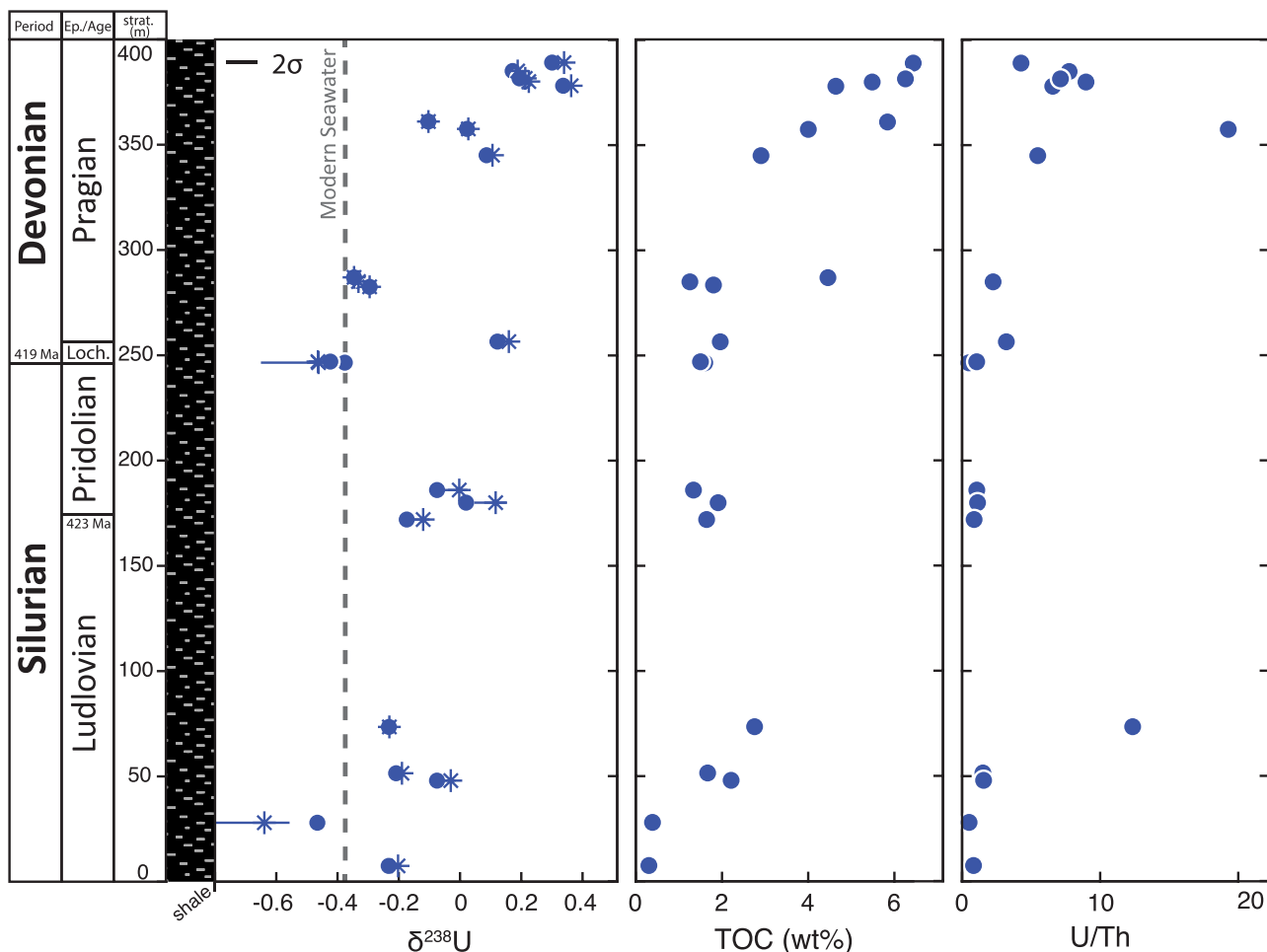


**Figure 6.** Uranium isotope, TOC, and U/Th data from ferruginous shale samples in the Road River Group at Tetlit Creek. All samples shown have iron speciation signatures consistent with deposition under a ferruginous water column ( $\text{Fe}_{\text{HR}}/\text{Fe}_{\text{T}} > 0.38$ ;  $\text{Fe}_{\text{PY}}/\text{Fe}_{\text{HR}} < 0.7$ ).  $\delta^{238}\text{U}$  and  $\delta^{238}\text{U}_{\text{auth}}$  data shown by circles and stars, respectively. Circles represent original data, while stars show  $\delta^{238}\text{U}_{\text{auth}}$  with error bars calculated based on confidence intervals for crustal input from Cole et al. (2017), while the 2 sigma error is the error on isotope measurements. The error on the TOC and U/Th measurements are smaller than the data points.

et al., 2008). Significantly, there is no evidence that sulfide should play a role as a U reductant in either of the lakes examined. Sulfide concentrations were below detection limits ( $1 \mu\text{M}$ ) at the time of sampling, and any available sulfide would immediately precipitate with plentiful Fe (II) as FeS—a reaction which has very fast kinetics (Rickard, 1995). While some FeS is likely present, and U (VI) removal via FeS has been demonstrated in laboratory experiments (Hua & Deng, 2008), this two-step process involving adsorption and subsequent slow and partial reduction has not been shown to be an important U removal pathway in natural settings (Chappaz et al., 2010).

Third, vivianite—a reduced iron-phosphate mineral—is saturated in the water column below 6–7 m depth throughout the year (Lambrecht et al., 2018). It has also been shown that U can be abiotically reduced by biogenic vivianite (Veeramani et al., 2011); however, while any fractionations associated with this process have not, to our knowledge, been explored, reduction is close to quantitative on a time scale of days, potentially leading to no expressed fractionations. Equally, incorporation of U into other phosphate minerals (e.g., carbonate fluorapatite) has not been found to result in a fractionation based on experimental results (Dang et al., 2016). Finally, there is also potential for changes in the available reductant or primary reduction pathways on short time scales during the course of deposition of these sediments. In sum, the complexity of this natural setting makes any conclusions about the reduction mechanisms difficult without additional work to untangle water residence time, U sources, and an age model for the sediment core.

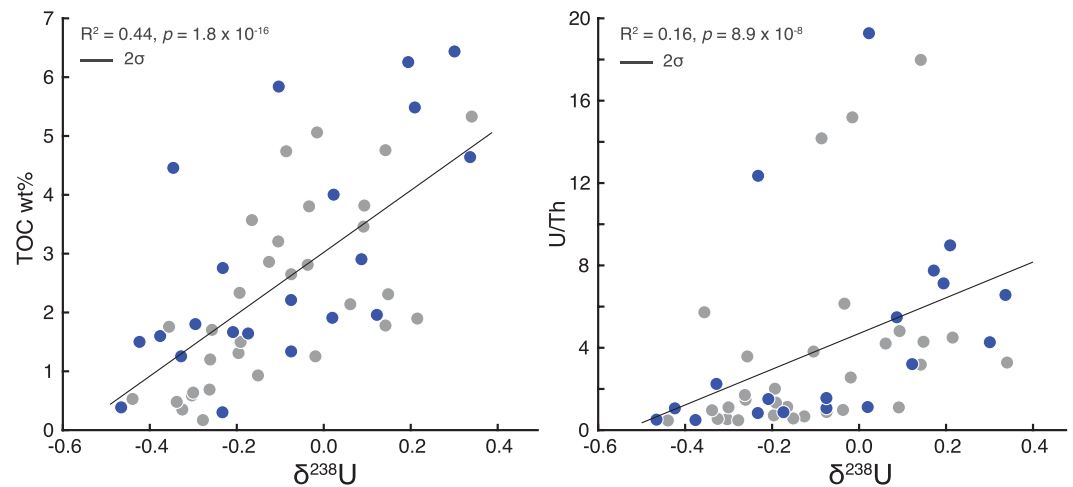


**Figure 7.** Uranium isotope data from all Paleozoic samples (Tetlit Creek; blue, and graptolite samples; gray) relative to TOC and U/Th. The  $2\sigma$  is the error on the  $\delta^{238}\text{U}$  measurements. The regression line is calculated using the measured values of  $\delta^{238}\text{U}$ , TOC wt%, and U/Th. All samples shown have iron speciation signatures consistent with deposition under a ferruginous water column ( $\text{Fe}_{\text{HR}}/\text{Fe}_{\text{T}} > 0.38$ ;  $\text{Fe}_{\text{PY}}/\text{Fe}_{\text{HR}} < 0.7$ ).

### 5.1.2. Lake Pavin

In Lake Pavin, there is no apparent relationship between the four cores with water depth, though both cores from near the chemocline trend toward lighter values with sediment depth. While this could be interpreted as progressive U reduction via ferrous iron in porewaters, a progressive increase in U/Th would also be expected, and this is not observed. In contrast, the core from 92 m trends toward heavier values below 10 cm depth. Although these data cannot be compared with sediments of comparable core depth from the other cores, the overall variability from both lakes is indicative of not only variable expression of fractionation factors, but also potential for reduction via multiple reduction pathways and, subsequently, rates of reduction (e.g., Brown et al., 2018). Similar to Brownie Lake, we do not expect any influence from sulfide reduction, as sulfide concentrations are controlled by the presence of Fe (II) and therefore extremely low in both the water column and sediment pore waters (Busigny et al., 2014).

As in Brownie Lake, we observe a lack of distinct isotopic signatures between sediments deposited above and below the chemocline; however, the specific processes behind our observed data are difficult to parse. Here we again address some key processes relevant to this environment and our observations. First, while the isotopic effects of microbial reduction that have been characterized in previous studies result in the preferential reduction of heavy U, it has also been experimentally demonstrated that abiotic reduction with ferrous iron can achieve the opposite effect, enriching reduced species in light U (Brown et al., 2018; Stylo et al., 2015). Additionally, it is possible that reduction via ferrous iron can be close to quantitative (Du et al., 2011), or not induce a fractionation (Rademacher et al., 2006), which would result in sediments with similar isotopic values to overlying waters. Second, vivianite is also present in Lake Pavin (Cosmidis et al., 2014), and as discussed above, this may provide an alternative pathway for U reduction in this and other ferruginous settings (Veeramani et al., 2011). Finally, there is also the potential for sorption of U to iron oxides—a process with a preference for light U (e.g., Weyer et al., 2008)—and subsequent reduction of this light pool occurring in either the water column or the sediment pile, often referred to as an “iron shuttle.” There is no evidence for preservation of iron oxides in the sediment column below oxic waters, which is expected given that they are highly organic-rich (Busigny et al., 2016). In sum, the data observed in both lakes would be best explained by a combination of the processes outlined above—given evidence of anoxic sediment core values both lighter and heavier than those of the oxic core. Although parsing the roles of each removal pathway is beyond the scope of this initial survey, this highlights that ferruginous settings are not simply sequestering heavy U as occurs in euxinic environments where microbial U reduction dominates (Andersen et al., 2014; Hinojosa et al., 2016; Noordmann et al., 2015; Rolison et al., 2017; Weyer et al., 2008).

## 5.2. Peru Margin

The Peru Margin OMZ is characterized by relatively muted  $\delta^{238}\text{U}$  fractionations relative to both the seawater and the core top sediments underlying the more oxygenated bottom waters below the OMZ ( $[\text{O}_2] > 50 \mu\text{M}$ ) (Scholz et al., 2016; Scholz et al., 2017). Within and at the edges of the OMZ, a range of suboxic to anoxic waters persist, resulting in strongly enriched TOC burial and trace metal accumulation within the OMZ (Böning et al., 2004) (Figure 5). It is reasonable to consider that such environments would likely be important components of the marine redox landscape earlier in Earth's history, coincident with increased anoxic area, or as environments that may be classified as ferruginous based on iron speciation yet lack high concentrations of Fe (II). The modest  $\delta^{238}\text{U}$  values observed in these sediments, as well as the lack of distinction between those within and below the OMZ, are in stark contrast to the canonical view of distinctive  $\delta^{238}\text{U}$  signatures from anoxic and oxic environments. Further, the Peru Margin OMZ sustains the highest U enrichments relative to other similar settings such as the Gulf of California, the Namibian Margin, and the Oman Margin (Böning et al., 2004) (Figure 5). This indicates that a nontrivial fraction of U reduction and removal from the marine system occurs in these environments and is associated with a muted isotopic fractionation from seawater. While we observe a relationship between U/Th and TOC ( $R^2 = 0.55$ ,  $p = 1.1 \times 10^{-5}$ ), as has been previously noted (McManus et al., 2005), this is not reflected in the isotopic record. Lastly, it should be noted that even in modern euxinic environments, U reduction occurs primarily in the sediment pile (e.g., Klinkhammer & Palmer, 1991)—therefore, it is unlikely that the U isotopic values from the Peru Margin merely reflect a shift to (deeper) sediment pile reduction (e.g., Clark & Johnson, 2008). That is, the muted apparent U isotope fractionation is likely not the result of sediment pile reduction being unique to this setting. Given that speciation effects should be similar in all modern seawater, these data may suggest dominance of a different reduction pathway, such as rapid and nearly quantitative reduction via ferrous iron in the uppermost (core-top) portion of the sediment pile (Du et al., 2011).

## 5.3. Silurian-Devonian Shales

### 5.3.1. Road River Group and Graptolitic Shale Samples

Using iron speciation, we have identified a continuous section of samples deposited under ferruginous conditions (see SI). Within this 400 m section (covering <20 Ma across the Silurian-Devonian boundary), we observe highly variable  $\delta^{238}\text{U}$  values ranging  $\sim 0.8\text{‰}$ , but also recording shifts of up to  $\sim 0.6\text{‰}$  within a 20–70 m interval (Figure 6). Some  $\delta^{238}\text{U}$  values exhibit stratigraphic jumps of 0.2–0.5‰ between samples only separated by 10–20 m of stratigraphy. A similar pattern is seen in the Cape Phillips Formation samples, where variance of 0.5‰ is recorded between samples from a single graptolite biozone. In the traditional U isotope mass balance framework, these would be interpreted as rapid shifts in global redox landscape. However, the problems with such an interpretation are twofold. First, the variability is unlikely to be primarily driven by shifts in global marine  $\delta^{238}\text{U}$  resulting from changes in the extent of reducing seafloor area, given the magnitude and frequency of shifts. Based on the range of  $\delta^{238}\text{U}$  observed in surface systems and our understanding of the U isotope mass balance, it would be impossible to shift marine  $\delta^{238}\text{U}$  to extreme isotopic values without observing a sharp drop in marine U concentrations (e.g., Lau et al., 2016), and there is no evidence for this from U/Th data. Second, given that these sediments have been constrained as ferruginous and, so far, in modern analog systems, we only find evidence for high variability instead of consistent, large, and unidirectional U isotope fractionations, we find no basis on which to attribute isotopic shifts in these Paleozoic sediments solely to changes in the seawater isotopic composition. The exception to this may be the broad trend toward heavier  $\delta^{238}\text{U}$  in the upper part of the Tetlit Creek section, which would lead traditional U isotope studies to suggest an expansion of oxic waters. Yet, equally, based on the evidence of this study, in the event of changing seawater isotopic values, the same trend could also be explained by a decrease in global euxinic area and/or an expansion of ferruginous environments. Lastly, and most importantly, we observe a significant relationship between TOC content and  $\delta^{238}\text{U}$  (Figure 7). Such a relationship between organic matter and  $\delta^{238}\text{U}$  has been previously observed in modern settings (Andersen et al., 2014; Severmann, 2015), and our findings show a similar dependence through the Tetlit Creek stratigraphy (Figure 6). This consistent stratigraphic trend would suggest that  $\delta^{238}\text{U}$  is most primarily tied to organic matter loading—a local effect—and as such, not the signature of a global shift.

Overall, we suggest that the most parsimonious interpretation of these data—and especially the rapid shifts on short stratigraphic scales—is variable expression of U isotope fractionations and reduction pathways in

this ferruginous environment, just as we have observed in the modern analog ferruginous and anoxic systems. The extent of fractionation from a given seawater value during reduction will be tied to both the reduction pathway (biotic, abiotic, or sorption-mediated removal and subsequent reduction) and open (water column) or closed (pore water) system behavior (e.g., Andersen et al., 2014; Andersen et al., 2017; Clark & Johnson, 2008). In addition, increased organic matter loading in the Tetlit Creek section tends to result in larger, positive U isotope fractionations. As in the lakes, there is also the likelihood that a given reduction pathway could produce a range of sedimentary  $\delta^{238}\text{U}$  values due to muted or fully expressed fractionations. For example, during reduction in the water column, the full isotopic fractionation associated with a given reduction pathway would be expected as U would not be diffusion limited. However, it should be noted that in modern environments, water column reduction only becomes important in very high productivity environments (Andersen et al., 2017). In contrast, reduction could occur in the pore waters of the sediment column, resulting in muted fractionations due to diffusion-limited U supply (Clark & Johnson, 2008), while partial reduction in the water column will further dampen subsequent U isotope fractionations in the sediment column.

The additional Ordovician-Devonian graptolitic shale samples, also identified as ferruginous based on iron speciation, echo the variability observed in the Tetlit Creek and Twilight Creek sections. Although these samples cannot be tied to trends in a given sedimentary section, these data similarly demonstrate the range of potential fractionations in a ferruginous environment. These samples also show a similar relationship between TOC and  $\delta^{238}\text{U}$ , again suggesting that increased organic matter loading may strongly contribute to expression of larger fractionations.

The majority of graptolitic shale values fall below 0‰; if we expect an isotopic fractionation from seawater in all anoxic settings of approximately +0.6‰ (e.g., Andersen et al., 2014), this would require seawater to be −0.6‰ or lighter during much of this timespan. Further, if we also account for the variability and the heaviest values observed (0.4‰), this would require that seawater cannot be more than ~0.2‰ lighter than modern. While such shifts between these two endmember scenarios may be possible on the timespan that these samples represent, we do not currently have a direct record of seawater  $\delta^{238}\text{U}$  against which to test an interpretation of major (order of magnitude) swings in reducing area. Instead, we suggest that the most parsimonious interpretation of this data is the same as all other sample sets in this study—variable expression of fractionation factors associated with reduction in ferruginous settings, organic matter loading, and UMAR.

Combining all Paleozoic data, we observe correlations between both  $\delta^{238}\text{U}$  and U/Th and  $\delta^{238}\text{U}$  and TOC (Figure 6). This suggests that the efficiency of reduction or higher rates of U accumulation are tied to larger effective fractionations. Interestingly, this is seemingly in contrast to what has been predicted experimentally (Brown et al., 2018). These heavier values resemble expected U isotope fractionations during microbially dominated U reduction in euxinic environments. Equally, these values may also simply reflect ancient ferruginous settings in which nonmicrobial U reduction was the predominant means of U sequestration (e.g., Hood et al., 2016). In addition to variation in  $\delta^{238}\text{U}$  values, there is nearly an order of magnitude variation in U/Th values in sediments deposited under similar redox conditions (as constrained by iron speciation; SI). While this may result from some heterogeneity in seawater U concentrations or restricted settings, this also reflects substantial variability in the accumulation or removal rates of U. This variability may be tied to organic matter loading, changes in sedimentation rate, the efficiency of reduction, or, most likely, a combination of these factors. This magnitude of variability in UMAR alone has the potential to substantially impact the outcome of isotope mass balance modeling results (Figure 9).

#### 5.4. Revisiting the Isotope Mass Balance

Here we use a global U isotope mass balance model to explore the potential influence of variation of both fractionation factor ( $\Delta^{238}\text{U}$ ) and UMAR in ferruginous settings on the reconstruction of global marine paleoredox conditions. In contrast to traditional approaches, we have included a separate ferruginous sink (table of parameters; SI). Because ferruginous settings would be the dominant reducing environment across the majority of Earth's history (e.g., Poulton & Canfield, 2011), inclusion of this sink is a critical component of any model when attempting to quantify the expanse of low oxygen conditions.

The model is initially set to sustain modern steady state using the mass balance and isotope mass balance of Dunk et al. (2002) and Tissot and Dauphas (2015). Because the modern system does not include any



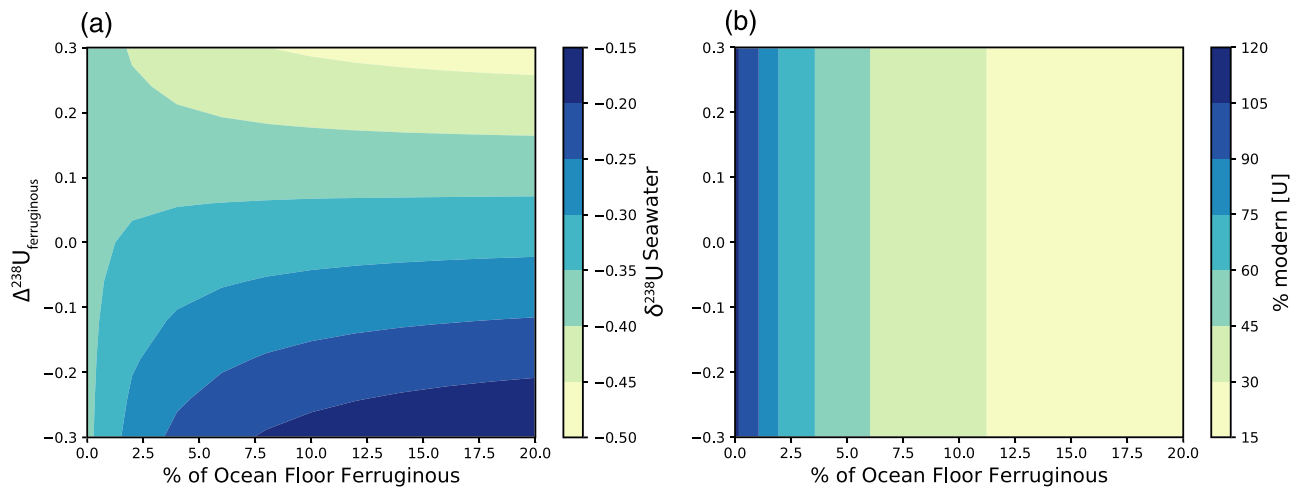


**Figure 8.** Isotope mass balance model outputs as result of varying  $\Delta^{238}\text{U}_{\text{ferr}}$  and area of ferruginous ocean floor. (a) Colorbar indicates  $\delta^{238}\text{U}$  value of seawater at steady state. (b) Colorbar indicates [U] in seawater expressed as a percentage of modern.

substantial ferruginous environments, the initial area of this sink is set to zero. We then perturb the system by increasing the ferruginous area and exploring the effects of varying the isotopic fractionation factor associated with this sink, as well as the efficiency of U burial in these environments. While it is likely that the extent of other reducing sinks will vary with expansion of ferruginous environments (e.g., expansion of suboxic regions), we solely consider variation related to ferruginous environments to more simply explore the influence of this added removal pathway.

#### 5.4.1. $\Delta^{238}\text{U}$ in Ferruginous Settings

The primary aim of this study was to provide constraints on  $\Delta^{238}\text{U}_{\text{ferr}}$  (effective fractionation in ferruginous environments); however, our data suggest that a large range of fractionations occur in natural ferruginous settings, and any single average would result in an oversimplification of the system. Building on this observation, we explore the effects on seawater  $\delta^{238}\text{U}$  values using an approximation of the range of  $\Delta^{238}\text{U}_{\text{ferr}}$  from our data ( $-0.3\text{‰}$  to  $+0.3\text{‰}$ ). We find that values close to modern seawater  $\delta^{238}\text{U}$  are sustained at almost any extent of ferruginous seafloor area if we use an average  $\Delta^{238}\text{U}_{\text{ferr}}$  of  $\sim 0.1$  (Figure 8a). Although [U] concentrations will drop substantially as this sink expands, as would be expected (Figure 8b), assessing this change in siliciclastic sediments would require both large temporal and global data sets as well as a high-resolution understanding of sediment accumulation rates. While we demonstrate this large solution space for given seawater  $\delta^{238}\text{U}$ , it is likely that the size of other sinks would also change in concert with a substantial increase in ferruginous seafloor area. We do not account for this likelihood, as this model is more representative of a thought experiment, although constraints from other proxies on the expanse of other environments that are substantial sinks for U may provide useful information to eliminate certain redox scenarios.

This expansion of the potential redox landscapes consistent with modern-like  $\delta^{238}\text{U}$  seawater values may also provide a resolution for conflicting data sets—particularly in the Paleozoic and Proterozoic. For example, Yang et al. (2017) suggest that reconstructed  $\delta^{238}\text{U}$  seawater values from 1.36 Ga sediments were within 0.1–0.3‰ of modern values and that such values indicate an ocean where <25% of the seafloor was anoxic—in other words, that the oceans had become largely ventilated relative to the majority of the Precambrian. However, given the framework presented here, this data set would be consistent not only with large areas of oxic or weakly oxygenated seafloor area as the authors have discussed but also with large areas of ferruginous seafloor. This interpretation would be precisely in line with the global marine landscape expected during this interval (Poulton & Canfield, 2011).

#### 5.4.2. Uranium Removal Efficiency

We also explore the effects of changes to UMAR. Uranium accumulation rates used in marine sinks in the isotope mass balance are calibrated using modern analogs—however, in reducing settings in the modern, these rates are strongly tied to organic matter loading and sedimentation rates (e.g., Dunk et al., 2002). Importantly, these settings are represented by small restricted basins (e.g., Cariaco Basin) and near-shore, high productivity regions (coastal upwelling regions). These types of reducing environments are

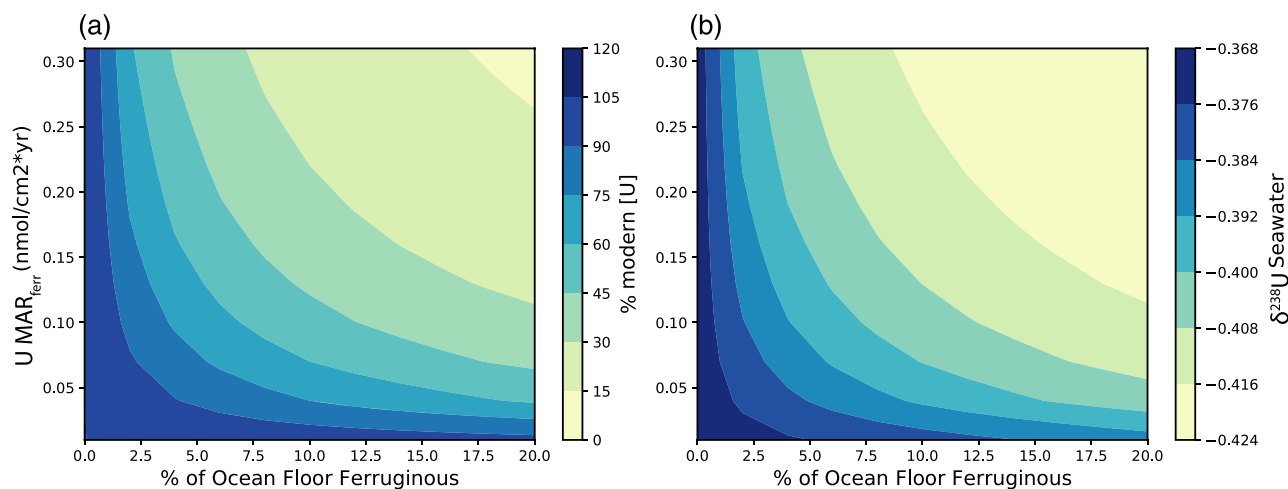


**Figure 9.** Isotope mass balance model outputs as a result of varying U MAR and area of ferruginous ocean floor. (a) Colorbar indicates [U] in seawater at steady state as a percentage of modern. (b) Colorbar indicates  $\delta^{238}\text{U}$  value of seawater at steady state.

characterized by high sediment and organic matter fluxes. In contrast, the distribution of reducing waters in a world with low atmospheric oxygen and poorly oxygenated deep oceans would be fundamentally different, with extensive distal reducing environments (e.g., through much of the Paleozoic and Precambrian; Wallace et al., 2017). In these deep sea settings, mean UMAR may have been much lower—tied closely to productivity and organic matter flux—as a result of much lower sedimentation rates (Crockford et al., 2018; Derry, 2015; Laakso & Schrag, 2014; Ozaki et al., 2019; Reinhard et al., 2017).

We have assessed the impact of lower UMAR by exploring an order of magnitude range of flux efficiencies, using modern values from reducing environments that sustain steady state as an upper limit. We consider this a reasonable upper limit, as the reducing settings of the modern ocean have high sulfate reduction rates, which scale linearly with rate of U reduction (Barnes & Cochran, 1993), and these rates would have been much lower prior to the eventual ocean ventilation in the Paleozoic. At rates about half as efficient as U removal in modern euxinic sinks, seawater [U] can remain within 20% of modern values with up to 5% of the ocean floor ferruginous (Figure 9a). Uranium MAR has a smaller impact on the isotopic mass balance, but changes in seawater  $\delta^{238}\text{U}$  can still be driven by UMAR alone with a fixed  $\Delta^{238}\text{U}_{\text{ferr}}$  (Figure 9b). Understanding the potential variation in the efficiency of ferruginous sinks is equally critical to identifying the associated isotopic fractionations in order to provide reasonable interpretations of U isotope data in the sedimentary record.

This model is not meant to reconstruct the redox environment in any given interval in Earth's history. Instead, we aim to highlight the size of the potential solution space for a given seawater  $\delta^{238}\text{U}$  value. While the extent of reducing seafloor area cannot be constrained as a result of isotopic variability observed in this study, it is possible that  $\delta^{238}\text{U}$  data could provide information on the extent of euxinic environments. Although there is some overlap in the isotopic fractionations that can be expressed in ferruginous and euxinic settings—particularly in conjunction with high TOC—consistently positive fractionations have been found in the modern euxinic settings examined thus far. Therefore, light seawater values may provide compelling evidence for extensive euxinic conditions, whereas heavy (near modern) seawater  $\delta^{238}\text{U}$  values can indicate either a well oxygenated or largely ferruginous ocean state, or any combination of these environments.

In sum, this framework suggests that near modern seawater  $\delta^{238}\text{U}$  values are consistent with limited euxinic seafloor area but do not necessarily suggest a well oxygenated marine environment. Indeed, near modern values through the Proterozoic—an interval expected to be dominated by ferruginous environments (e.g., Planavsky et al., 2011; Poulton & Canfield, 2011)—may confirm that euxinia was very rare (Reinhard et al., 2013). Further, distinct negative excursions in the  $\delta^{238}\text{U}$  seawater record (e.g., Lau et al., 2016; Wei et al., 2018; Zhang, Romaniello, et al., 2018; Zhang, Xiao, et al., 2018) may provide more compelling evidence for an expansion of euxinic environments, rather than just low oxygen environments.

## 6. Concluding Remarks

Evidence from both modern analogs and Paleozoic ferruginous sediments alike show that the  $\delta^{238}\text{U}$  signature for reduction in ferruginous environments is highly variable. In our examined modern ferruginous settings,  $\delta^{238}\text{U}$  values are indistinguishable from adjacent oxic settings. This is consistent with the influence of both reduction rate and competing isotope effects (negative kinetic fractionations versus positive NVE fractionations) in defining the values preserved in the sedimentary record. As a result, it is difficult to suggest that a given seawater  $\delta^{238}\text{U}$  value can be interpreted uniquely in terms of the amount of oxic versus anoxic seafloor area. Our study forces acknowledgment of a much larger solution space in global U isotope mass balance models than typically considered for a given  $\delta^{238}\text{U}$  data set; however, this may help to resolve conflicting interpretations of the redox environment in the Proterozoic and Paleozoic. While this conclusion does not undermine the idea that extremely light seawater  $\delta^{238}\text{U}$  is indicative of substantial portions of anoxic (likely euxinic) depositional area (e.g., Lau et al., 2016; Wei et al., 2018; Zhang, Algeo, et al., 2018), we demonstrate that it is possible to maintain  $\delta^{238}\text{U}$  seawater values similar to the modern even in a largely ferruginous ocean.

## Data Availability Statement

All data generated for this study are included in the Supplementary Information, along with additional contextual information for rock samples. Data archiving is in compliance with FAIR data guidelines, and the data set for this study can be found at DOI: 10.5281/zenodo.3901758

## Acknowledgments

We thank Dr. Alf Lenz for generously providing Tetlit Creek and Twilight Creek graptolitic shale samples. We thank Tessa Browne, Una Farrell, and Joe Malinowski for laboratory assistance. We thank Paige Bauer, Nick Lambrecht, and Duncan Widman for assistance in the field. E. A. S. acknowledges funding from a Sloan Ocean Sciences Research Fellowship and the Stanford Program on Deepwater Depositional Systems for support. NSF EAR-1660691 to E. D. S. and EAR-1660761 to C. W. supported Brownie Lake work. V. B. acknowledges funding from the National Program of Planetology (PNP) 2015 of the Institut National des Sciences de l'Univers and the UnivEarths Labex program at Sorbonne Paris Cité (ANR-10-LABX-0023 and ANR-11-IDEX-0005-02). N. J. P. acknowledges support from the Alternative Earth's NASA Astrobiology Institute.

## References

- Abe, M., Hada, M., Suzuki, T., Fujii, Y., & Hirao, K. (2014). Theoretical study of isotope enrichment caused by nuclear volume effect. *Journal of Computer Chemistry, Japan*, 13(1), 92–104. <https://doi.org/10.2477/jccj.2013-0015>
- Abe, M., Suzuki, T., Fujii, Y., & Hada, M. (2008). An ab initio study based on a finite nucleus model for isotope fractionation in the U (III)–U (IV) exchange reaction system. *The Journal of Chemical Physics*, 128(14), 144309. <https://doi.org/10.1063/1.2898541>
- Abe, M., Suzuki, T., Fujii, Y., Hada, M., & Hirao, K. (2008). An ab initio molecular orbital study of the nuclear volume effects in uranium isotope fractionations. *The Journal of Chemical Physics*, 129(16), 164309. <https://doi.org/10.1063/1.2992616>
- Abe, M., Suzuki, T., Fujii, Y., Hada, M., & Hirao, K. (2010). Ligand effect on uranium isotope fractionations caused by nuclear volume effects: An ab initio relativistic molecular orbital study. *The Journal of Chemical Physics*, 133(4), 044309. <https://doi.org/10.1063/1.3463797>
- Andersen, M. B., Elliott, T., Freymuth, H., Sims, K. W., Niu, Y., & Kelley, K. A. (2015). The terrestrial uranium isotope cycle. *Nature*, 517(7534), 356–359. <https://doi.org/10.1038/nature14062>
- Andersen, M. B., Romaniello, S., Vance, D., Little, S. H., Herdman, R., & Lyons, T. W. (2014). A modern framework for the interpretation of  $^{238}\text{U}/^{235}\text{U}$  in studies of ancient ocean redox. *Earth and Planetary Science Letters*, 400, 184–194. <https://doi.org/10.1016/j.epsl.2014.05.051>
- Andersen, M. B., Stirling, C. H., & Weyer, S. (2017). Uranium isotope fractionation. *Reviews in Mineralogy and Geochemistry*, 82(1), 799–850. <https://doi.org/10.2138/rmg.2017.82.19>
- Andersen, M. B., Vance, D., Morford, J. L., Bura-Nakić, E., Breitenbach, S. F. M., & Och, L. (2016). Closing in on the marine  $^{238}\text{U}/^{235}\text{U}$  budget. *Chemical Geology*, 420, 11–22. <https://doi.org/10.1016/j.chemgeo.2015.10.041>
- Anderson, T. F., & Raiswell, R. (2004). Sources and mechanisms for the enrichment of highly reactive iron in euxinic Black Sea sediments. *American Journal of Science*, 304(3), 203–233. <https://doi.org/10.2475/ajs.304.3.203>
- Barnes, C. E., & Cochran, J. K. (1993). Uranium geochemistry in estuarine sediments: Controls on removal and release processes. *Geochimica et Cosmochimica Acta*, 57(3), 555–569. [https://doi.org/10.1016/0016-7037\(93\)90367-6](https://doi.org/10.1016/0016-7037(93)90367-6)
- Bartlett, R., Elrick, M., Wheeley, J. R., Polyak, V., Desrochers, A., & Asmerom, Y. (2018). Abrupt global-ocean anoxia during the Late Ordovician–early Silurian detected using uranium isotopes of marine carbonates. *Proceedings of the National Academy of Sciences*, 115(23), 5896–5901. <https://doi.org/10.1073/pnas.1802438115>
- Basu, A., Brown, S. T., Christensen, J. N., DePaolo, D. J., Reimus, P. W., Heikoop, J. M., et al. (2015). Isotopic and geochemical tracers for U (VI) reduction and U mobility at an in situ recovery U mine. *Environmental Science & Technology*, 49(10), 5939–5947. <https://doi.org/10.1021/acs.est.5b00701>
- Basu, A., Sanford, R. A., Johnson, T. M., Lundstrom, C. C., & Löffler, F. E. (2014). Uranium isotopic fractionation factors during U (VI) reduction by bacterial isolates. *Geochimica et Cosmochimica Acta*, 136, 100–113. <https://doi.org/10.1016/j.gca.2014.02.041>
- Bigeleisen, J. (1996a). Nuclear size and shape effects in chemical reactions. Isotope chemistry of the heavy elements. *Journal of the American Chemical Society*, 118(15), 3676–3680. <https://doi.org/10.1021/ja954076k>
- Bigeleisen, J. (1996b). Temperature dependence of the isotope chemistry of the heavy elements. *Proceedings of the National Academy of Sciences*, 93(18), 9393–9396. <https://doi.org/10.1073/pnas.93.18.9393>
- Bigeleisen, J., & Mayer, M. G. (1947). Calculation of equilibrium constants for isotopic exchange reactions. *The Journal of Chemical Physics*, 15(5), 261–267. <https://doi.org/10.1063/1.1746492>
- Böning, P., Brumsack, H.-J., Böttcher, M. E., Schnetger, B., Kriete, C., Kallmeyer, J., & Borchers, S. L. (2004). Geochemistry of Peruvian near-surface sediments. *Geochimica et Cosmochimica Acta*, 68(21), 4429–4451. <https://doi.org/10.1016/j.gca.2004.04.027>
- Bopp, C. J. IV, Lundstrom, C. C., Johnson, T. M., Sanford, R. A., Long, P. E., & Williams, K. H. (2010). Uranium  $^{238}\text{U}/^{235}\text{U}$  isotope ratios as indicators of reduction: Results from an in situ biostimulation experiment at Rifle, Colorado, USA. *Environmental Science & Technology*, 44(15), 5927–5933. <https://doi.org/10.1021/es100643v>

- Brennecke, G. A., Herrmann, A. D., Algeo, T. J., & Anbar, A. D. (2011). Rapid expansion of oceanic anoxia immediately before the end-Permian mass extinction. *Proceedings of the National Academy of Sciences*, *108*(43), 17631–17634. <https://doi.org/10.1073/pnas.1106039108>
- Brennecke, G. A., Wasylenko, L. E., Bargar, J. R., Weyer, S., & Anbar, A. D. (2011). Uranium isotope fractionation during adsorption to Mn-oxyhydroxides. *Environmental Science & Technology*, *45*(4), 1370–1375. <https://doi.org/10.1021/es103061v>
- Brown, S. T., Basu, A., Ding, X., Christensen, J. N., & DePaolo, D. J. (2018). Uranium isotope fractionation by abiotic reductive precipitation. *Proceedings of the National Academy of Sciences*, *115*. <https://doi.org/10.1073/pnas.1805234115>
- Busigny, V., Jézéquel, D., Cosmidis, J., Viollier, E., Benzerara, K., Planavsky, N. J., et al. (2016). The Iron Wheel in Lac Pavin: Interaction with phosphorus cycle. In *Lake Pavin*, edited, (pp. 205–220). Switzerland: Springer.
- Busigny, V., Planavsky, N. J., Jézéquel, D., Crowe, S., Louvat, P., Moureau, J., et al. (2014). Iron isotopes in an Archean ocean analogue. *Geochimica et Cosmochimica Acta*, *133*, 443–462. <https://doi.org/10.1016/j.gca.2014.03.004>
- Canfield, D. E., Poulton, S. W., Knoll, A. H., Narbonne, G. M., Ross, G., Goldberg, T., & Strauss, H. (2008). Ferruginous conditions dominated later Neoproterozoic deep-water chemistry. *Science*, *321*(5891), 949–952. <https://doi.org/10.1126/science.1154499>
- Canfield, D. E., Raiswell, R., Westrich, J. T., Reaves, C. M., & Berner, R. A. (1986). The use of chromium reduction in the analysis of reduced inorganic sulfur in sediments and shales. *Chemical Geology*, *54*(1–2), 149–155. [https://doi.org/10.1016/0009-2541\(86\)90078-1](https://doi.org/10.1016/0009-2541(86)90078-1)
- Canfield, D. E., & Thamdrup, B. (2009). Towards a consistent classification scheme for geochemical environments, or, why we wish the term ‘suboxic’ would go away. *Geobiology*, *7*(4), 385–392. <https://doi.org/10.1111/j.1472-4669.2009.00214.x>
- Chappaz, A., Gobeil, C., & Tessier, A. (2010). Controls on uranium distribution in lake sediments. *Geochimica et Cosmochimica Acta*, *74*(1), 203–214. <https://doi.org/10.1016/j.gca.2009.09.026>
- Clark, S. K., & Johnson, T. M. (2008). Effective isotopic fractionation factors for solute removal by reactive sediments: A laboratory microcosm and slurry study. *Environmental Science & Technology*, *42*(21), 7850–7855. <https://doi.org/10.1021/es801814v>
- Clarkson, M. O., Stirling, C. H., Jenkyns, H. C., Dickson, A. J., Porcelli, D., Moy, C. M., et al. (2018). Uranium isotope evidence for two episodes of deoxygenation during Oceanic Anoxic Event 2. *Proceedings of the National Academy of Sciences*, *115*. <https://doi.org/10.1073/pnas.1715278115>
- Clarkson, M. O., Wood, R. A., Poulton, S. W., Richoz, S., Newton, R. J., Kasemann, S. A., et al. (2016). Dynamic anoxic ferruginous conditions during the end-Permian mass extinction and recovery. *Nature Communications*, *7*(1), 12,236. <https://doi.org/10.1038/ncomms12236>
- Cole, D. B., Mills, D. B., Erwin, D. H., Sperling, E. A., Porter, S. M., Reinhard, C. T., & Planavsky, N. J. (2020). On the co-evolution of surface oxygen levels and animals. *Geobiology*, *18*(3), 260–281. <https://doi.org/10.1111/gbi.12382>
- Cole, D. B., Zhang, S., & Planavsky, N. J. (2017). A new estimate of detrital redox-sensitive metal concentrations and variability in fluxes to marine sediments. *Geochimica et Cosmochimica Acta*, *215*, 337–353. <https://doi.org/10.1016/j.gca.2017.08.004>
- Cosmidis, J., Benzerara, K., Morin, G., Busigny, V., Lebeau, O., Jézéquel, D., et al. (2014). Biomineralization of iron-phosphates in the water column of Lake Pavin (Massif Central, France). *Geochimica et Cosmochimica Acta*, *126*, 78–96. <https://doi.org/10.1016/j.gca.2013.10.037>
- Crockford, P. W., Hayles, J. A., Bao, H., Planavsky, N. J., Bekker, A., Fralick, P. W., et al. (2018). Triple oxygen isotope evidence for limited mid-Proterozoic primary productivity. *Nature*, *559*(7715), 613–616. <https://doi.org/10.1038/s41586-018-0349-y>
- Dang, D. H., Novotnik, B., Wang, W., Georg, R. B., & Evans, R. D. (2016). Uranium isotope fractionation during adsorption, (co) precipitation, and biotic reduction. *Environmental Science & Technology*, *50*(23), 12695–12704. <https://doi.org/10.1021/acs.est.6b01459>
- Derry, L. A. (2015). Causes and consequences of mid-Proterozoic anoxia. *Geophysical Research Letters*, *42*, 8538–8546. <https://doi.org/10.1002/2015GL065333>
- Du, X., Boonchayaanant, B., Wu, W.-M., Fendorf, S., Bargar, J., & Criddle, C. S. (2011). Reduction of uranium (VI) by soluble iron (II) conforms with thermodynamic predictions. *Environmental Science & Technology*, *45*(11), 4718–4725. <https://doi.org/10.1021/es2006012>
- Dunk, R. M., Mills, R. A., & Jenkins, W. J. (2002). A reevaluation of the oceanic uranium budget for the Holocene. *Chemical Geology*, *190*(1–4), 45–67. [https://doi.org/10.1016/S0009-2541\(02\)00110-9](https://doi.org/10.1016/S0009-2541(02)00110-9)
- Elrick, M., Polyak, V., Algeo, T. J., Romaniello, S., Asmerom, Y., Herrmann, A. D., et al. (2017). Global-ocean redox variation during the middle-late Permian through Early Triassic based on uranium isotope and Th/U trends of marine carbonates. *Geology*, *45*(2), 163–166. <https://doi.org/10.1130/G38585.1>
- Fakrae, M., & Katsev, S. (2019). Organic sulfur was integral to the Archean sulfur cycle. *Nature Communications*, *10*(1), 1–8. <https://doi.org/10.1038/s41467-019-12396-y>
- Fujii, Y., Higuchi, N., Haruno, Y., Nomura, M., & Suzuki, T. (2006). Temperature dependence of isotope effects in uranium chemical exchange reactions. *Journal of Nuclear Science and Technology*, *43*(4), 400–406. <https://doi.org/10.1080/18811248.2006.9711111>
- Fujii, Y., Nomura, M., Okamoto, M., Onitsuka, H., Kawakami, F., & Takeda, K. (1989). An anomalous isotope effect of  $^{235}\text{U}$  in U (IV)-U (VI) chemical exchange. *Zeitschrift für Naturforschung A*, *44*(5), 395–398. <https://doi.org/10.1515/zna-1989-0507>
- Fujii, Y., Nomura, M., Onitsuka, H., & Takeda, K. (1989). Anomalous isotope fractionation in uranium enrichment process. *Journal of Nuclear Science and Technology*, *26*(11), 1061–1064. <https://doi.org/10.1080/18811248.1989.9734427>
- Gilleaudeau, G. J., Romaniello, S. J., Luo, G., Kaufman, A. J., Zhang, F., Kläbe, R. M., et al. (2019). Uranium isotope evidence for limited euxinia in mid-Proterozoic oceans. *Earth and Planetary Science Letters*, *521*, 150–157. <https://doi.org/10.1016/j.epsl.2019.06.012>
- Gueguen, B., Reinhard, C. T., Algeo, T. J., Peterson, L. C., Nielsen, S. G., Wang, X., et al. (2016). The chromium isotope composition of reducing and oxic marine sediments. *Geochimica et Cosmochimica Acta*, *184*, 1–19. <https://doi.org/10.1016/j.gca.2016.04.004>
- Guilbaud, R., Poulton, S. W., Butterfield, N. J., Zhu, M., & Shields-Zhou, G. A. (2015). A global transition to ferruginous conditions in the early Neoproterozoic oceans. *Nature Geoscience*, *8*(6), 466–470. <https://doi.org/10.1038/ngeo2434>
- Gutiérrez, D., Enríquez, E., Purca, S., Quipúzcoa, L., Marquina, R., Flores, G., & Graco, M. (2008). Oxygenation episodes on the continental shelf of central Peru: Remote forcing and benthic ecosystem response. *Progress in Oceanography*, *79*(2–4), 177–189. <https://doi.org/10.1016/j.pocean.2008.10.025>
- Halevy, I., Alesker, M., Schuster, E., Popovitz-Biro, R., & Feldman, Y. (2017). A key role for green rust in the Precambrian oceans and the genesis of iron formations. *Nature Geoscience*, *10*(2), 135–139. <https://doi.org/10.1038/ngeo2878>
- Hiess, J., Condon, D. J., McLean, N., & Noble, S. R. (2012).  $^{238}\text{U}/^{235}\text{U}$  systematics in terrestrial uranium-bearing minerals. *Science*, *335*(6076), 1610–1614. <https://doi.org/10.1126/science.1215507>
- Hinojosa, J. L., Stirling, C. H., Reid, M. R., Moy, C. M., & Wilson, G. S. (2016). Trace metal cycling and  $^{238}\text{U}/^{235}\text{U}$  in New Zealand’s fjords: Implications for reconstructing global paleoredox conditions in organic-rich sediments. *Geochimica et Cosmochimica Acta*, *179*, 89–109. <https://doi.org/10.1016/j.gca.2016.02.006>
- Holland, H. D. (1984). *The chemical evolution of the atmosphere and oceans*. Princeton, NJ: Princeton University Press.

- Hood, A. v., Planavsky, N. J., Wallace, M. W., Wang, X., Bellefroid, E. J., Gueguen, B., & Cole, D. B. (2016). Integrated geochemical-petrographic insights from component-selective  $\delta^{238}\text{U}$  of Cryogenian marine carbonates. *Geology*, *44*(11), 935–938. <https://doi.org/10.1130/G38533.1>
- Hua, B., & Deng, B. (2008). Reductive immobilization of uranium (VI) by amorphous iron sulfide. *Environmental Science & Technology*, *42*(23), 8703–8708. <https://doi.org/10.1021/es801225z>
- Jackson, D. E., & Lenz, A. (1962). Zonation of Ordovician and Silurian graptolites of northern Yukon, Canada. *AAPG Bulletin*, *46*(1), 30–45. <https://doi.org/10.1306/bc743757-16be-11d7-8645000102c1865d>
- Kendall, B., Creaser, R. A., Reinhard, C. T., Lyons, T. W., & Anbar, A. D. (2015). Transient episodes of mild environmental oxygenation and oxidative continental weathering during the late Archean. *Science Advances*, *1*(10), e1500777. <https://doi.org/10.1126/sciadv.1500777>
- Klinkhammer, G. P., & Palmer, M. R. (1991). Uranium in the oceans: Where it goes and why. *Geochimica et Cosmochimica Acta*, *55*(7), 1799–1806. [https://doi.org/10.1016/0016-7037\(91\)90024-Y](https://doi.org/10.1016/0016-7037(91)90024-Y)
- Ku, T.-L., Knauss, K. G., & Mathieu, G. G. (1977). Uranium in open ocean: Concentration and isotopic composition. *Deep Sea Research*, *24*(11), 1005–1017. [https://doi.org/10.1016/0146-6291\(77\)90571-9](https://doi.org/10.1016/0146-6291(77)90571-9)
- Kudrass, H. (2000). *Cruise report SO147 Peru Upwelling: Valparaiso-Callao, 29.05.–03.07. 2000*. Hannover, Germany: BGR Hannover.
- Laakso, T. A., & Schrag, D. P. (2014). Regulation of atmospheric oxygen during the Proterozoic. *Earth and Planetary Science Letters*, *388*, 81–91. <https://doi.org/10.1016/j.epsl.2013.11.049>
- Lambrech, N., Wittkop, C., Katsev, S., Fakhraee, M., & Swanner, E. D. (2018). Geochemical characterization of two ferruginous meromictic lakes in the Upper Midwest, USA. *Journal of Geophysical Research: Biogeosciences*, *123*, 3403–3422. <https://doi.org/10.1029/2018JG004587>
- Lau, K. V., Lyons, T. W., & Maher, K. (2020). Uranium reduction and isotopic fractionation in reducing sediments: Insights from reactive transport modeling. *Geochimica et Cosmochimica Acta*. <https://doi.org/10.1016/j.gca.2020.01.021>
- Lau, K. V., Macdonald, F. A., Maher, K., & Payne, J. L. (2017). Uranium isotope evidence for temporary ocean oxygenation in the aftermath of the Sturtian Snowball Earth. *Earth and Planetary Science Letters*, *458*, 282–292. <https://doi.org/10.1016/j.epsl.2016.10.043>
- Lau, K. V., Maher, K., Altiner, D., Kelley, B. M., Kump, L. R., Lehmann, D. J., et al. (2016). Marine anoxia and delayed Earth system recovery after the end-Permian extinction. *Proceedings of the National Academy of Sciences*, *113*(9), 2360–2365. <https://doi.org/10.1073/pnas.1515080113>
- Lenton, T. M., Boyle, R. A., Poulton, S. W., Shields-Zhou, G. A., & Butterfield, N. J. (2014). Co-evolution of eukaryotes and ocean oxygenation in the Neoproterozoic era. *Nature Geoscience*, *7*(4), 257–265. <https://doi.org/10.1038/ngeo2108>
- Lenz, A. C. (1988). Upper Silurian and Lower Devonian graptolites and graptolite biostratigraphy, northern Yukon, Canada. *Canadian Journal of Earth Sciences*, *25*(3), 355–369. <https://doi.org/10.1139/e88-039>
- Lenz, A. C. (2013). Early Devonian graptolites and graptolite biostratigraphy, Arctic Islands, Canada. *Canadian Journal of Earth Sciences*, *50*(11), 1097–1115. <https://doi.org/10.1139/cjes-2013-0057>
- Lu, X., Kendall, B., Stein, H. J., Li, C., Hannah, J. L., Gordon, G. W., & Ebbestad, J. O. R. (2017). Marine redox conditions during deposition of Late Ordovician and Early Silurian organic-rich mudrocks in the Siljan ring district, central Sweden. *Chemical Geology*, *457*, 75–94. <https://doi.org/10.1016/j.chemgeo.2017.03.015>
- Lückge, A., & Reinhardt, L. (2000). CTD measurements in the water column off Peru. In *Cruise report SO147 Peru Upwelling: Valparaiso-Callao, 29.05.-03.07* (pp. 35–37). Hannover, Germany: Fed. Inst. for Geosci. and Nat. Resour.(BRG).
- Lyons, T. W., & Gill, B. C. (2010). Ancient sulfur cycling and oxygenation of the early biosphere. *Elements*, *6*(2), 93–99. <https://doi.org/10.2113/gselements.6.2.93>
- März, C., Poulton, S., Beckmann, B., Küster, K., Wagner, T., & Kasten, S. (2008). Redox sensitivity of P cycling during marine black shale formation: Dynamics of sulfidic and anoxic, non-sulfidic bottom waters. *Geochimica et Cosmochimica Acta*, *72*(15), 3703–3717. <https://doi.org/10.1016/j.gca.2008.04.025>
- McManus, J., Berelson, W. M., Klinkhammer, G. P., Hammond, D. E., & Holm, C. (2005). Authigenic uranium: Relationship to oxygen penetration depth and organic carbon rain. *Geochimica et Cosmochimica Acta*, *69*(1), 95–108. <https://doi.org/10.1016/j.gca.2004.06.023>
- Meyer, K. M., & Kump, L. R. (2008). Oceanic euxinia in Earth history: Causes and consequences. *Annual Review of Earth and Planetary Sciences*, *36*(1), 251–288. <https://doi.org/10.1146/annurev.earth.36.031207.124256>
- Michard, G., Viollier, E., Jézéquel, D., & Sarazin, G. (1994). Geochemical study of a crater lake: Pavin Lake, France—Identification, location and quantification of the chemical reactions in the lake. *Chemical Geology*, *115*(1-2), 103–115. [https://doi.org/10.1016/0009-2541\(94\)90147-3](https://doi.org/10.1016/0009-2541(94)90147-3)
- Minneapolis Parks & Recreation Board. (2017). *Water resources report, City of Minneapolis Public Works*. Minneapolis: City of Minneapolis Public Works.
- Montoya-Pino, C., Weyer, S., Anbar, A. D., Pross, J., Oschmann, W., van de Schootbrugge, B., & Arz, H. W. (2010). Global enhancement of ocean anoxia during Oceanic Anoxic Event 2: A quantitative approach using U isotopes. *Geology*, *38*(4), 315–318. <https://doi.org/10.1130/G30652.1>
- Murphy, M. J., Stirling, C. H., Kaltenbach, A., Turner, S. P., & Schaefer, B. F. (2014). Fractionation of  $^{238}\text{U}/^{235}\text{U}$  by reduction during low temperature uranium mineralisation processes. *Earth and Planetary Science Letters*, *388*, 306–317. <https://doi.org/10.1016/j.epsl.2013.11.034>
- Noffke, A., Hensen, C., Sommer, S., Scholz, F., Bohlen, L., Mosch, T., et al. (2012). Benthic iron and phosphorus fluxes across the Peruvian oxygen minimum zone. *Limnology and Oceanography*, *57*(3), 851–867. <https://doi.org/10.4319/lo.2012.57.3.0851>
- Nomura, M., Higuchi, N., & Fujii, Y. (1996). Mass dependence of uranium isotope effects in the U (IV)–U (VI) exchange reaction. *Journal of the American Chemical Society*, *118*(38), 9127–9130. <https://doi.org/10.1021/ja954075s>
- Noordmann, J., Weyer, S., Montoya-Pino, C., Dellwig, O., Neubert, N., Eckert, S., et al. (2015). Uranium and molybdenum isotope systematics in modern euxinic basins: Case studies from the central Baltic Sea and the Kyllaren fjord (Norway). *Chemical Geology*, *396*, 182–195. <https://doi.org/10.1016/j.chemgeo.2014.12.012>
- Ozaki, K., Reinhard, C. T., & Tajika, E. (2019). A sluggish mid-Proterozoic biosphere and its effect on Earth's redox balance. *Geobiology*, *17*(1), 3–11. <https://doi.org/10.1111/gbi.12317>
- Planavsky, N. J., McGoldrick, P., Scott, C. T., Li, C., Reinhard, C. T., Kelly, A. E., et al. (2011). Widespread iron-rich conditions in the mid-Proterozoic ocean. *Nature*, *477*(7365), 448–451. <https://doi.org/10.1038/nature10327>
- Plass, A., Schlosser, C., Sommer, S., Dale, A. W., Achterberg, E. P., & Scholz, F. (2019). The control of hydrogen sulfide on benthic iron and cadmium fluxes in the oxygen minimum zone off Peru. *Biogeosciences Discussions*, *2019*, 1–52. <https://doi.org/10.5194/bg-2019-390>
- Poulton, S. W., & Canfield, D. E. (2005). Development of a sequential extraction procedure for iron: Implications for iron partitioning in continentally derived particulates. *Chemical Geology*, *214*(3–4), 209–221. <https://doi.org/10.1016/j.chemgeo.2004.09.003>

- Poulton, S. W., & Canfield, D. E. (2011). Ferruginous conditions: A dominant feature of the ocean through Earth's history. *Elements*, 7(2), 107–112. <https://doi.org/10.2113/gselements.7.2.107>
- Poulton, S. W., Fralick, P. W., & Canfield, D. E. (2010). Spatial variability in oceanic redox structure 1.8 billion years ago. *Nature Geoscience*, 3(7), 486–490. <https://doi.org/10.1038/ngeo889>
- Poulton, S. W., Henkel, S., März, C., Urquhart, H., Flögel, S., Kasten, S., et al. (2015). A continental-weathering control on orbitally driven redox-nutrient cycling during Cretaceous Oceanic Anoxic Event 2. *Geology*, 43(11), 963–966. <https://doi.org/10.1130/G36837.1>
- Rademacher, L. K., Lundstrom, C. C., Johnson, T. M., Sanford, R. A., Zhao, J., & Zhang, Z. (2006). Experimentally determined uranium isotope fractionation during reduction of hexavalent U by bacteria and zero valent iron. *Environmental Science & Technology*, 40(22), 6943–6948. <https://doi.org/10.1021/es0604360>
- Raiswell, R., & Canfield, D. E. (1998). Sources of iron for pyrite formation in marine sediments. *American Journal of Science*, 298(3), 219–245. <https://doi.org/10.2475/ajs.298.3.219>
- Reinhard, C. T., Planavsky, N. J., Gill, B. C., Ozaki, K., Robbins, L. J., Lyons, T. W., et al. (2017). Evolution of the global phosphorus cycle. *Nature*, 541(7637), 386–389. <https://doi.org/10.1038/nature20772>
- Reinhard, C. T., Planavsky, N. J., Robbins, L. J., Partin, C. A., Gill, B. C., Lalonde, S. V., et al. (2013). Proterozoic ocean redox and biogeochemical stasis. *Proceedings of the National Academy of Sciences*, 110(14), 5357–5362. <https://doi.org/10.1073/pnas.1208622110>
- Revsbech, N. P., Larsen, L. H., Gundersen, J., Dalsgaard, T., Ulloa, O., & Thamdrup, B. (2009). Determination of ultra-low oxygen concentrations in oxygen minimum zones by the STOX sensor. *Limnology and Oceanography: Methods*, 7(5), 371–381. <https://doi.org/10.4319/lom.2009.7.371>
- Rickard, D. (1995). Kinetics of FeS precipitation: Part 1. Competing reaction mechanisms. *Geochimica et Cosmochimica Acta*, 59(21), 4367–4379. [https://doi.org/10.1016/0016-7037\(95\)00251-T](https://doi.org/10.1016/0016-7037(95)00251-T)
- Rimmer, S. M. (2004). Geochemical paleoredox indicators in Devonian–Mississippian black shales, Central Appalachian Basin (USA). *Chemical Geology*, 206(3–4), 373–391. <https://doi.org/10.1016/j.chemgeo.2003.12.029>
- Rolison, J. M., Stirling, C. H., Middag, R., & Rijkenberg, M. J. A. (2017). Uranium stable isotope fractionation in the Black Sea: Modern calibration of the  $^{238}\text{U}/^{235}\text{U}$  paleo-redox proxy. *Geochimica et Cosmochimica Acta*, 203, 69–88. <https://doi.org/10.1016/j.gca.2016.12.014>
- Rudnick, R., & Gao, S. (2014). Composition of the continental crust. In H. D. Holland, & K. K. Turekian (Eds.), *Treatise on geochemistry* (pp. 1–51). Oxford: Elsevier. <https://doi.org/10.1016/B978-0-08-095975-7.00301-6>
- Sageman, B. B., Murphy, A. E., Werne, J. P., Ver Straeten, C. A., Hollander, D. J., & Lyons, T. W. (2003). A tale of shales: The relative roles of production, decomposition, and dilution in the accumulation of organic-rich strata, Middle–Upper Devonian, Appalachian basin. *Chemical Geology*, 195(1–4), 229–273. [https://doi.org/10.1016/S0009-2541\(02\)00397-2](https://doi.org/10.1016/S0009-2541(02)00397-2)
- Schauble, E. A. (2007). Role of nuclear volume in driving equilibrium stable isotope fractionation of mercury, thallium, and other very heavy elements. *Geochimica et Cosmochimica Acta*, 71(9), 2170–2189. <https://doi.org/10.1016/j.gca.2007.02.004>
- Scholz, F., Löscher, C. R., Fiskal, A., Sommer, S., Hensen, C., Lomnitz, U., et al. (2016). Nitrate-dependent iron oxidation limits iron transport in anoxic ocean regions. *Earth and Planetary Science Letters*, 454, 272–281. <https://doi.org/10.1016/j.epsl.2016.09.025>
- Scholz, F., Siebert, C., Dale, A. W., & Frank, M. (2017). Intense molybdenum accumulation in sediments underneath a nitrogenous water column and implications for the reconstruction of paleo-redox conditions based on molybdenum isotopes. *Geochimica et Cosmochimica Acta*, 213, 400–417. <https://doi.org/10.1016/j.gca.2017.06.048>
- Severmann, S. (2015). Uranium stable isotopes: A proxy for productivity or ocean oxygenation? In *Paper Presented at AGU Fall Meeting Abstracts*. San Francisco: AGU.
- Shiel, A., Johnson, T. M., Lundstrom, C. C., Laubach, P., Long, P., & Williams, K. (2016). Reactive transport of uranium in a groundwater bioreduction study: Insights from high-temporal resolution  $^{238}\text{U}/^{235}\text{U}$  data. *Geochimica et Cosmochimica Acta*, 187, 218–236. <https://doi.org/10.1016/j.gca.2016.05.020>
- Sperling, E. A., Knoll, A. H., & Girguis, P. R. (2015). The ecological physiology of Earth's second oxygen revolution. *Annual Review of Ecology, Evolution, and Systematics*, 46(1), 215–235. <https://doi.org/10.1146/annurev-ecolsys-110512-135808>
- Sperling, E. A., Wolock, C. J., Morgan, A. S., Gill, B. C., Kunzmann, M., Halverson, G. P., et al. (2015). Statistical analysis of iron geochemical data suggests limited late Proterozoic oxygenation. *Nature*, 523(7561), 451–454. <https://doi.org/10.1038/nature14589>
- Stirling, C. H., Andersen, M. B., Potter, E.-K., & Halliday, A. N. (2007). Low-temperature isotopic fractionation of uranium. *Earth and Planetary Science Letters*, 264(1–2), 208–225. <https://doi.org/10.1016/j.epsl.2007.09.019>
- Stirling, C. H., Andersen, M. B., Warthmann, R., & Halliday, A. N. (2015). Isotope fractionation of  $^{238}\text{U}$  and  $^{235}\text{U}$  during biologically-mediated uranium reduction. *Geochimica et Cosmochimica Acta*, 163, 200–218. <https://doi.org/10.1016/j.gca.2015.03.017>
- Stockey, R. G., Cole, D. B., Planavsky, N. J., Loydell, D. K., Fryda, J., & Sperling, E. A. (2020). Persistent global marine euxinia in the early Silurian. *Nature Communications*, 11(1), 1804. <https://doi.org/10.1038/s41467-020-15400-y>
- Stokey, L. L. (1970). Ferrozine—A new spectrophotometric reagent for iron. *Analytical Chemistry*, 42(7), 779–781. <https://doi.org/10.1021/ac60289a016>
- Stylo, M., Neubert, N., Wang, Y., Monga, N., Romaniello, S. J., Weyer, S., & Bernier-Latmani, R. (2015). Uranium isotopes fingerprint biotic reduction. *Proceedings of the National Academy of Sciences*, 112(18), 5619–5624. <https://doi.org/10.1073/pnas.1421841112>
- Thamdrup, B., Dalsgaard, T., & Revsbech, N. P. (2012). Widespread functional anoxia in the oxygen minimum zone of the Eastern South Pacific. *Deep Sea Research Part I: Oceanographic Research Papers*, 65, 36–45. <https://doi.org/10.1016/j.dsr.2012.03.001>
- Tissot, F. L. H., & Dauphas, N. (2015). Uranium isotopic compositions of the crust and ocean: Age corrections, U budget and global extent of modern anoxia. *Geochimica et Cosmochimica Acta*, 167, 113–143. <https://doi.org/10.1016/j.gca.2015.06.034>
- Tracey, B., Lee, N., & Card, V. (1996). Sediment indicators of meromixis: Comparison of laminations, diatoms, and sediment chemistry in Brownie Lake, Minneapolis, USA. *Journal of Paleolimnology*, 15(2), 129–132. <https://doi.org/10.1007/bf00196776>
- Vedamati, J., Goepfert, T., & Moffett, J. W. (2014). Iron speciation in the eastern tropical South Pacific oxygen minimum zone off Peru. *Limnology and Oceanography*, 59(6), 1945–1957. <https://doi.org/10.4319/lo.2014.59.6.1945>
- Veeramani, H., Alessi, D. S., Suvorova, E. I., Lezama-Pacheco, J. S., Stubbs, J. E., Sharp, J. O., et al. (2011). Products of abiotic U (VI) reduction by biogenic magnetite and vivianite. *Geochimica et Cosmochimica Acta*, 75(9), 2512–2528. <https://doi.org/10.1016/j.gca.2011.02.024>
- Viollier, E., Jézéquel, D., Michard, G., Pèpe, M., Sarazin, G., & Alberic, P. (1995). Geochemical study of a crater lake (Pavin Lake, France): Trace-element behaviour in the monimolimnion. *Chemical Geology*, 125(1–2), 61–72. [https://doi.org/10.1016/0009-2541\(95\)00059-U](https://doi.org/10.1016/0009-2541(95)00059-U)
- Wallace, M. W., Hood, A. V., Shuster, A., Greig, A., Planavsky, N. J., & Reed, C. P. (2017). Oxygenation history of the Neoproterozoic to early Phanerozoic and the rise of land plants. *Earth and Planetary Science Letters*, 466, 12–19. <https://doi.org/10.1016/j.epsl.2017.02.046>
- Wang, X., Johnson, T. M., & Lundstrom, C. C. (2015). Isotope fractionation during oxidation of tetravalent uranium by dissolved oxygen. *Geochimica et Cosmochimica Acta*, 150, 160–170. <https://doi.org/10.1016/j.gca.2014.12.007>

- Wang, X., Planavsky, N. J., Hofmann, A., Saupe, E. E., de Corte, B. P., Philippot, P., et al. (2018). A Mesoproterozoic shift in uranium isotope systematics. *Geochimica et Cosmochimica Acta*, 238, 438–452. <https://doi.org/10.1016/j.gca.2018.07.024>
- Wang, X., Planavsky, N. J., Reinhard, C. T., Hein, J. R., & Johnson, T. M. (2016). A Cenozoic seawater redox record derived from  $^{238}\text{U}/^{235}\text{U}$  in ferromanganese crusts. *American Journal of Science*, 316(1), 64–83. <https://doi.org/10.2475/01.2016.02>
- Wei, G.-Y., Planavsky, N. J., Tarhan, L., Chen, X., Wei, W., La, D., & Ling, H.-F. (2018). Marine redox fluctuation as a potential trigger for the Cambrian explosion. *Geology*, 46(7), 587–590. <https://doi.org/10.1130/G40150.1>
- Weyer, S., Anbar, A. D., Gerdes, A., Gordon, G. W., Algeo, T. J., & Boyle, E. A. (2008). Natural fractionation of  $^{238}\text{U}/^{235}\text{U}$ . *Geochimica et Cosmochimica Acta*, 72(2), 345–359. <https://doi.org/10.1016/j.gca.2007.11.012>
- White, D. A., Elrick, M., Romaniello, S., & Zhang, F. (2018). Global seawater redox trends during the Late Devonian mass extinction detected using U isotopes of marine limestones. *Earth and Planetary Science Letters*, 503, 68–77. <https://doi.org/10.1016/j.epsl.2018.09.020>
- Yang, S., Kendall, B., Lu, X., Zhang, F., & Zheng, W. (2017). Uranium isotope compositions of mid-Proterozoic black shales: Evidence for an episode of increased ocean oxygenation at 1.36Ga and evaluation of the effect of post-depositional hydrothermal fluid flow. *Precambrian Research*, 298, 187–201. <https://doi.org/10.1016/j.precamres.2017.06.016>
- Zhang, F., Algeo, T. J., Romaniello, S., Cui, Y., Zhao, L., Chen, Z.-Q., & Anbar, A. D. (2018). Congruent Permian-Triassic  $\delta^{238}\text{U}$  records at Panthalassic and Tethyan sites: Confirmation of global-oceanic anoxia and validation of the U-isotope paleoredox proxy. *Geology*, 46(4), 327–330. <https://doi.org/10.1130/G39695.1>
- Zhang, F., Romaniello, S. J., Algeo, T. J., Lau, K. V., Clapham, M. E., Richoz, S., et al. (2018). Multiple episodes of extensive marine anoxia linked to global warming and continental weathering following the latest Permian mass extinction. *Science Advances*, 4(4), e1602921. <https://doi.org/10.1126/sciadv.1602921>
- Zhang, F., Xiao, S., Kendall, B., Romaniello, S. J., Cui, H., Meyer, M., et al. (2018). Extensive marine anoxia during the terminal Ediacaran Period. *Science Advances*, 4(6), ean8983. <https://doi.org/10.1126/sciadv.aan8983>